A comprehensive kinetic model of the electronbeamexcited xenon chloride laser

Thomas H. Johnson, Harry E. Cartland, Thomas C. Genoni, and Allen M. Hunter

Citation: Journal of Applied Physics **66**, 5707 (1989); doi: 10.1063/1.343639
View online: http://dx.doi.org/10.1063/1.343639
View Table of Contents: http://scitation.aip.org/content/aip/journal/jap/66/12?ver=pdfcov
Published by the AIP Publishing

A comprehensive kinetic model of the electron-beam-excited xenon chloride laser

Thomas H. Johnson, Harry E. Cartland, Thomas C. Genoni,[a] and Allen M. Hunter[b]
Science Research Laboratory, U. S. Military Academy, West Point, New York 10996-5000

(Received 5 May 1989; accepted for publication 9 August 1989)

A new kinetics model capable of simulating performance of electron-beam-pumped xenon chloride lasers over the full range of experimental evidence is presented. The model comprises 202 chemical processes employing 41 species. Its operation is described and the full set of rate equations given. Calculations of stimulated emission and absorption cross sections for XeCl are presented, and simulations of various lasing results are shown in the context of explicating dominant processes. Major kinetics issues are examined, particularly those leading to the model's rates for vibrational excitation of HCl and for electron quenching of the excited excimer molecule.

I. INTRODUCTION

The kinetic processes determining the performance and scaling characteristics of the xenon chloride (XeCl) excimer laser have proved to be particularly difficult to specify in detail. While comprehensive models for both krypton fluoride and xenon fluoride have existed for some time, and although early attempts at modeling XeCl were indeed made,[1,2] a formulation that accurately reflects the diversity of existing data has thus far proved elusive. This paper proposes such a comprehensive model, and compares its predictions to the results of both lasing and kinetics experiments.

Initial lasing experiments in XeCl were conducted using Cl_2 as the chlorine donor; because of strong ground-state absorption by Cl_2, it was replaced in most later experiments by HCl. Buffer gases of both argon (at roughly 2 atm) and neon (at roughly 4 atm) have been used, and electron-beam (*e*-beam) pumped experiments have been conducted over a broad range of energy depositions, from below 0.1 to 6 MW/cm^3.[4–9] Intrinsic (local) efficiencies of laser operation have varied in these experiments over a range 4%–7%, with the shorter-pulse experiments generally being more efficient, although individual differences in devices have tended to dominate systematic tendencies in the relatively sparse data set. More reliable performance differences between the argon and neon buffers do appear. The most sensitive scaling parameter in lasing experiments is the variance of power out with initial HCl concentration, so the data on this variance has been one locus of interest.

Although previous kinetics models could approximate lasing output for short-pulse, high-pump-rate conditions, those same models could not equally well simulate long-pulse conditions. It has become evident that the minimum set of kinetic processes necessary to represent XeCl performance is both larger and more complex than the set required for other excimers, such as krypton fluoride.[10] These problems have been exacerbated, rather than simplified, by experiments[11–14] designed to study particular chemical kinetic parameters.

As was the case with krypton fluoride, many of the reaction rates of potential significance in XeCl mixtures are not known from direct experiment, but are either inferred, estimated by analogy, or approximated with *ab initio* computer calculations. Since many processes matter only in second order and since lasing results may not be terribly sensitive to factor-of-2 uncertainties even in many first-order processes, these uncertainties have not prevented development of accurate predictive models for KrF. The sheer number of processes relevant to XeCl does not necessarily suggest that the situation should be different once key problems are understood. Attention has focused for some time on the electron kinetics, both in relation to the electronic manifold of atomic xenon, and the chemistry of the halogen donor. Analyses using the XeCl model presented here suggest that the electron-HCl chemistry is indeed critical to understanding the behavior of kinetics experiments, and by extension of lasing as well.

In Sec. II we discuss the structure of the excited xenon chloride molecule and present results of our calculations of the stimulated emission and absorption cross sections; details are given in the Appendix. Section III summarizes the principal kinetic pathways in XeCl, highlighting differences with other rare gas-halide excimers, and presents simulations of lasing experiments. In Sec. IV, the full kinetic model is presented, with explanatory comments. In Sec. V, major individual kinetics issues underlying the model are discussed in some detail, with simulations of relevant experiments.

II. STIMULATED EMISSION AND ABSORPTION

The precise value of the stimulated emission cross section, and the corresponding value of the lower-state absorption cross section, remain uncertain. This section and the Appendix discuss the values chosen for this kinetic model.

The experimental data relevant to the stimulated emission cross section for XeCl* falls into two categories: fluorescence spectra[22] and gain spectra.[23] Early in the development of this model, an estimate for the stimulated emission cross section of 4.2 Å^2 was made by fitting a Lorentzian line profile to the gain spectrum of Bourne and Alcock.[23] The fluorescence spectrum offers a more valid basis for estimating the stimulated emission cross section since it involves only the upper state; gain spectra derive from the difference between the upper state and the lower state, and are subject to line

[a] Present address: Mission Research Corporation, Albuquerque, NM.
[b] Present address: Thermo Electron Technologies Corporation, San Diego, CA.

 0021-8979/89/245707-19$02.40

narrowing. The fluorescence data of Adamovich *et al.*[22] have the highest resolution, and thus are judged the best basis for estimating the stimulated emission cross section.

An estimate of the peak cross section can be made by making use of the relation

$$\sigma(\lambda) = \frac{\lambda^4}{8\pi c\tau}\frac{f(\lambda)}{k}, \tag{1}$$

where $f(\lambda)$ is the intensity in arbitrary units and

$$k = \int f(\lambda)d\lambda \tag{2}$$

is the integrated line shape. From the data in Ref. 22, we estimate an upper bound for the peak ($V' = 0 \rightarrow V'' = 2$) stimulated emission cross section at 308 nm of 5.0–5.6 Å^2, depending on exactly how the background contribution is included. This effectively bounds the range of practical (vibrationally averaged) values of the cross section.

We have also performed a theoretical calculation of the emission and absorption spectra. A schematic of the XeCl potential energy curves is shown in Fig. 1, identifying the lasing transition, $B(^2\Sigma) \rightarrow X(^2\Sigma)$. Of particular importance is the fact that the ground state is bound by 255 cm^{-1}, requiring the calculation of an absorption coefficient and raising the possibility of bottlenecking (see Sec. V).

In the kinetics calculations described in the following sections, we make no distinction between vibrational levels of the B and X states; that is, we track only the total state populations, denoted N_B and N_X. Our expression for the gain is, accordingly,

$$g = N_B\bar{\sigma}_S - N_X\bar{\sigma}_A, \tag{3}$$

where $\bar{\sigma}_S$ and $\bar{\sigma}_A$ are suitably defined as the average stimulated emission and absorption cross sections.

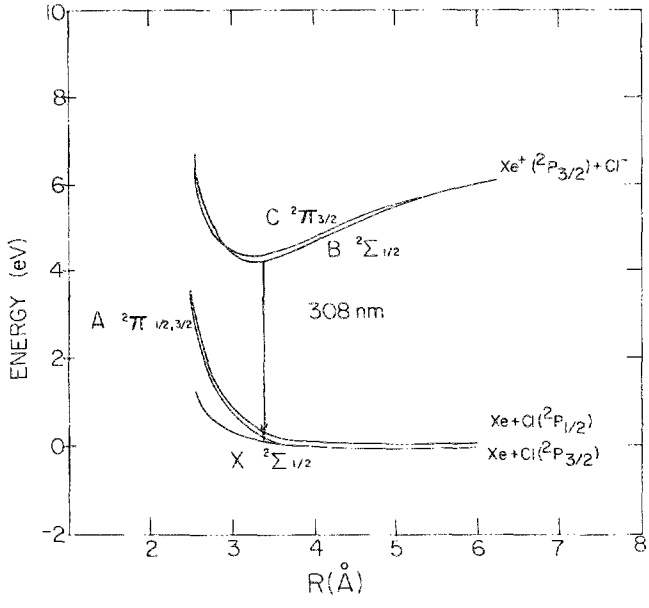

FIG. 1. Potential energy curves for the XeCl molecule. The upper laser level is the ionic $^2\Sigma$ state labeled B; the lower laser level is the covalent $^2\Sigma$ state labeled X. The B state is collisionally mixed with the ionic $^2\Pi$ C state, which can lase to the repulsive $^2\Pi$ A state.

A general expression for the gain as a function of wave number ν is given by

$$g(\nu) \cong \frac{\lambda^2}{8\pi\tau}\sum_{V'}\sum_{V''}\sum_{e,f}\sum_{J'}(J'+1)S(\nu-\tilde{\nu})(N_{V'J'} - N_{V''J''})$$

(P branch)

$$+\frac{\lambda^2}{8\pi\tau}\sum_{V'}\sum_{V''}\sum_{e,f}\sum_{J'}(J')S(\nu-\tilde{\nu})(N_{V'J'} - N_{V''J''})$$

(R branch), (4)

where λ is the wavelength, $\tau = 11$ ns is the measured raidative lifetime of the XeCl (B) state,[15] e and f refer to the two spin components for each transition, and $N_{V'J'}$, $N_{V''J''}$ are the B and X state number densities. The line shape S for a particular transition centered at $\tilde{\nu}$ is

$$S(\nu-\tilde{\nu}) = \frac{\Delta}{\pi c}\frac{\mathrm{FCF}}{(\nu-\tilde{\nu})^2 + \Delta^2}, \tag{5}$$

where FCF is the Franck–Condon factor and the linewidth $\Delta \simeq 0.1$ cm^{-1}/atm for rotational lines. Although the B state angular momentum coupling most closely resembles Hund's case c, the B-X transition has a strong $\Sigma \rightarrow \Sigma$ character as in XeF,[19] and we approximate the transition strengths for the P and R branches by the $\Sigma \rightarrow \Sigma$ values.[18]

Comparing (3) and (4), and assuming that the vibrational and rotational level populations are in thermal equilibrium, we see that appropriate definitions for $\sigma_S(\nu)$ and $\sigma_A(\nu)$ are

$$Q'\sigma_s(\nu) = \frac{\lambda^2}{8\pi\tau}\sum_{V'}\sum_{V''}\sum_{e,f}\sum_{J'}\sum_{P,R}\begin{bmatrix} J'+1 \\ J' \end{bmatrix} \times S(\nu-\tilde{\nu})e^{-E'/kT} \tag{6}$$

and

$$Q''\sigma_A(\nu) = \frac{\lambda^2}{8\pi\tau}\sum_{V'}\sum_{V''}\sum_{e,f}\sum_{J'}\sum_{P,R}\begin{bmatrix} J'+1 \\ J' \end{bmatrix} \times S(\nu-\tilde{\nu})e^{-E''/kT}, \tag{7}$$

where Q' and Q'' are the partition functions for the B and X states, respectively. Details of the calculation of $\sigma_S(\nu)$ and $\sigma_A(\nu)$ are given in the Appendix. Results are shown in Fig. 2. The peak value near the center of the 0-2 transition is approximately 4.8 Å^2.

As is obvious from Fig. 2, the emission line profile of

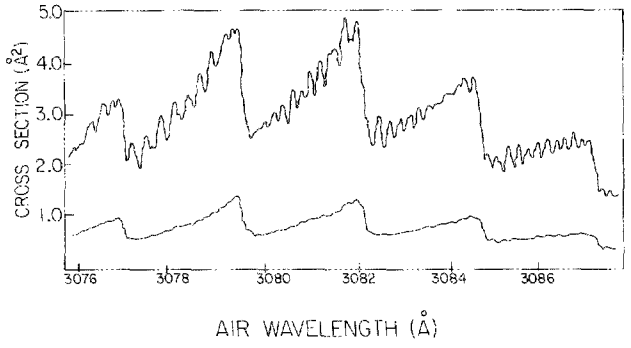

FIG. 2. Calculated values of XeCl stimulated emission (upper curve) and absorption (lower curve) cross sections near 308 nm.

XeCl* has significant structure. The laser experiments that we have simulated are relatively broadband and often display lasing on more than one line; for instance, the experiments at TTC[8] measured strong simultaneous lasing on both the $V' = 0 \rightarrow V'' = 2$ and the $V' = 0 \rightarrow V'' = 1$ transitions. Thus it is appropriate to use a spectral average for the stimulated emission cross section. The average cross section $\bar{\sigma}_s$ is smaller than the peak cross section by some 10%–15%. Hence, we have continued to find our initial estimate of 4.2 $Å^2$ to be a reasonable choice; a similar average determined the effective absorption cross section to be 1.2 $Å^2$. Such an average is difficult to define precisely, and could vary somewhat from experiment to experiment. Nevertheless, these particular values do agree with both data and calculations; their choice is supported by the excellence of the accuracy of laser performance simulations over a wide range of lasing conditions.

III. BASIC PROCESSES

XeCl chemistry differs from that of KrF primarily in the dominant pumping channels. In KrF the principal ion channel is the neutralization reaction of Kr^+ and F^-, with much of the Kr^+ having been produced in two-body charge transfer reactions with buffer gas ions; the principal neutral channel is harpooning of F_2 by metastable Kr atoms. But neither of these processes works well in XeCl because of the character of xenon: the two-body charge transfer rates from both Ne^+ and Ar^+ (and their molecular ions) to Xe are roughly two orders of magnitude below similar processes for krypton, and singly excited xenon (Xe*) does not have enough energy to form XeCl* with the preferred halogen donor, HCl. For some time it was thought that complex neutral channel reactions, depending mainly upon dissociative recombination of rare-gas molecular ions, would be necessary to explain the efficient flow of energy from the deposited e beam to XeCl* molecules. In 1980, however, a measurement by Collins and Lee[24] demonstrated efficient charge transfer to Xe from the Ar and Ne molecular ions in three-body processes, making it clear that the bulk of the energy could flow directly through the ions without direct involvement of secondary electron processes and metastable chemistry.

Figure 3 shows the main processes of this ion channel, the principal pumping pathways of XeCl*, in a neon buffer gas. Most of the electron-beam pump energy is deposited into neon ions, with a substantial fraction of the remainder going into Ne* metastables. The neon atomic ions are converted extremely rapidly (2 ns or less) to Ne_2^+ by three-body processes. At this point, the molecular ions may transfer their change to xenon atoms (as mentioned above, xenon is generally present as a few-Torr constituent in nominally 4 atm of neon or 2 atm of argon), neutralize Cl^- ions, or dissociatively recombine with electrons to produce Ne^{**} metastables. The latter two processes then channel energy to $XeCl^*$, since the molecule $NeCl^*$ predissociates. In an argon buffer, the processes are similar, except that neutralization of both Ar^+ and Ar_2^+ form $ArCl^*$, which can also lead to $XeCl^*$ through a displacement reaction.

Figure 4 shows a comparison, with representative reaction times, for energy flow options out of Ne_2^+, illustrating the efficiency of the ion channel over pumping through Cl^*. Since the lifetime of Ne_2^+ against dissociative recombination with electrons is on the order of 60 ns, it cannot compete with the other two principal processes and is not shown. Figure 5 shows that section of the ion chain peculiar to the argon buffer. Note that formation of $ArCl^*$ is slower than alternative pathways, and that once formed $ArCl^*$ is more likely to radiate than to lead to $XeCl^*$ through displacement of the argon by xenon. As a result, this displacement channel accounts for only a few percent of the total pumping in argon buffers even under the best of circumstances.

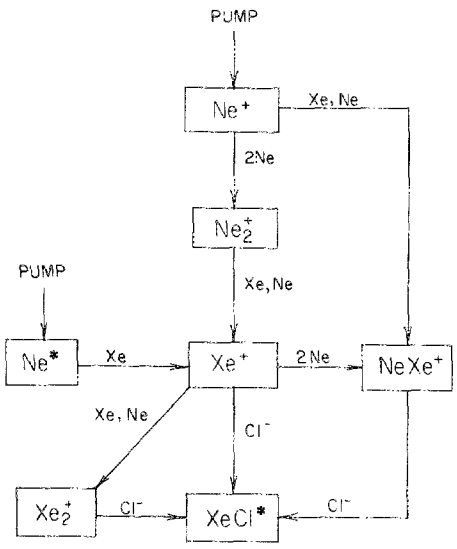

FIG. 3. Principal ion channel pumping of XeCl* in a neon buffer gas.

Figure 6 shows the major constituent reactions involved in neutral pumping. Apart from the Cl* channel already discussed, it will be immediately apparent why the neutral channel is less efficient than the ion channel: pumping requires that the energy flow through species (Xe^+, $NeXe^+$, and Xe_2^+) that are the primary paths in the ion channel. Neutral pumping then requires additional steps, involving electron reactions, in place of the fast (< 10 ns) neutraliza-

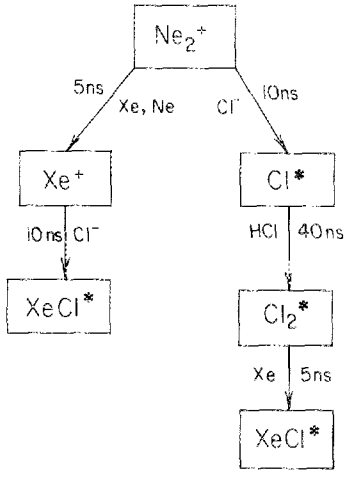

FIG. 4. Relative reaction times for pathways out of the neon molecular ion (times are calculated for 4 atm of neon buffer and representative values of other species concentrations).

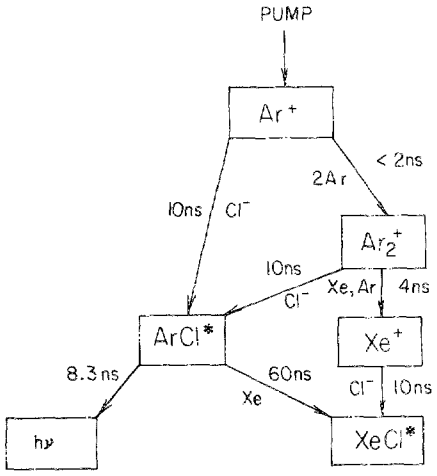

FIG. 5. Argon ion reactions and displacement channel pumping.

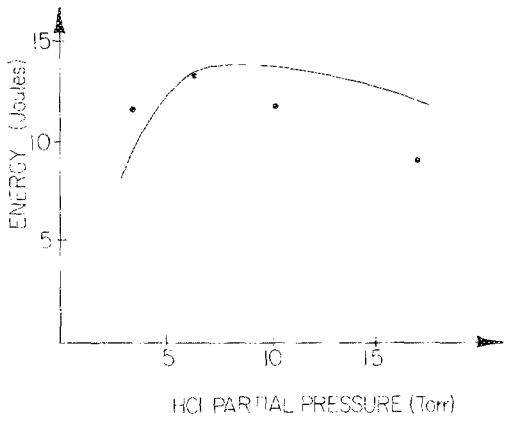

FIG. 7. Data (points) and model simulations (solid line) for laser energy out (joules) vs initial HCl concentration (Torr) in the Sandia experiments (Ref. 4). The experiments were conducted using an argon buffer gas and high pump power ($\simeq$3 MW/cm^3).

tion reaction of the ion channel; these electron rates are all much slower (generally 60–100 ns).

Secondary electron processes are, however, critical to the pumping. Of course, electrons are required to supply Cl^- through dissociative attachment. But unlike F_2, HCl has a very low cross section for attachment at low electron energies.[25] Exciting the first vibrational mode (roughly 2800 cm^{-1}) of HCl by electron impact increases the attachment cross section by a factor of 40; and exciting the second vibrational mode increases attachment by a factor of 800 over the ground-state cross section.[26] The critical question is then at what rate the HCl is vibrationally excited by secondary electrons, a question not settled simply by measurement of the cross sections for such excitations. This question is so complex and important that we reserve its discussion for a later section of this paper (Sec. V). The combined rate constants for excitation and attachment have themselves only a secondary influence on the depletion of HCl and the production of $XeCl^*$ through the ion neutralization channel, since for low rate constants the electron density will be higher. However, because the electron density is subject to other competing processes, and because the instantaneous species density of a major absorber (Cl^-) depends very sensitively on this rate, laser performance in most pumping regimes can be greatly affected by differences in overall attachment arising from differences in HCl vibrational excitation.

The relatively low rate of HCl excitation is one of the keys to the present model's ability to deal successfully with the scaling of output power with HCl partial pressure in both high- and low-pump-rate regimes. Examples of this success are shown in Figs. 7–9. Figure 7 shows data and the model's simulation results (using actual temporal e-beam pulse shapes) for the high-pump-rate (3 MW/cm^3), short-pulse (80 ns) regime of the Sandia experiments.[27] Only four data points exist for this scaling; although laser power appears to fall off faster with increasing HCl concentration than the model predicts, the differential at the two higher data points still lies within the experimental uncertainty.[28] An intermediate case is represented by the data and simulation from lasing experiments at Thermo Electron Technologies Corp. (formerly Western Research Corp.)[29] shown in Fig. 8. The figure shows the pulse shape for a single run of the TTC large aperture (40 cm$\times$40 cm) device, which was divided into four subapertures; the device was pumped at an average of roughly 350 kW/cm^3 for 600 ns. For this particular run, conducted with a 3.75-atm neon buffer and 2.5 Torr of HCl, the measured energy out was 979 J and the model's prediction was 1185 J. The experiment was conducted with a 10% mechanical obscuration of the output window, and the four apertures were shown to be differentially pumped, with two subapertures receiving weaker pumping. Neither of these effects was considered in the simulation. The agreement is thus better than might at first appear; corrected for the obscuration, the simulation is only 9% above the measurement. Further, this particular case represented not the simulation's best performance, but its worst (or, conversely, the experimental run with the worst nonuniformity of pumping). Figure 9 shows four different runs exploring the scaling of lasing power with HCl concentration, and the model's simulation of that scaling. In this plot, the simulation's results have been reduced by 10% to account for the obscuration, but differential pumping is not modeled. As with other results in both

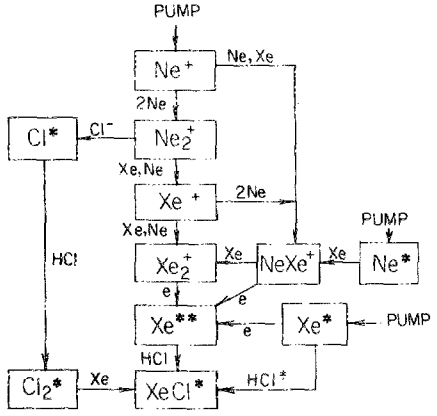

FIG. 6. Principal neutral channel pumping of XeCl* in a neon buffer gas.

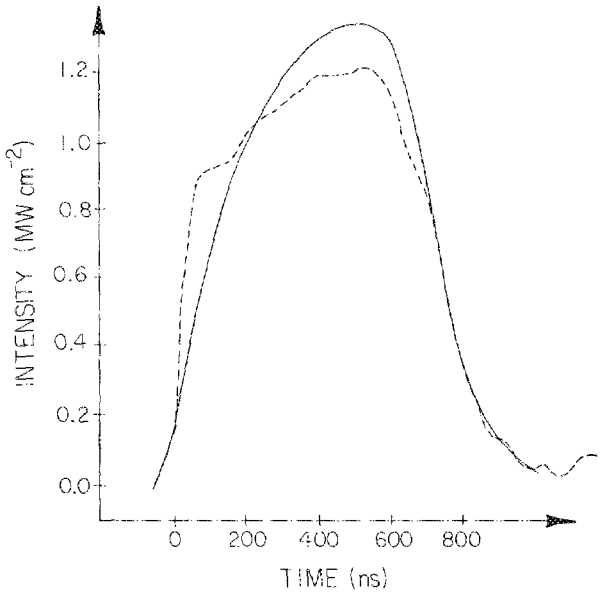

FIG. 8. Data (dashed curve) and model simulations (solid line) for laser pulseshape (intensity in MW/cm^2 vs time in ns) in an experiment conducted at Thermo Electron Technologies Corporation (Ref. 8). The buffer gas was neon, the pump power moderate ($\simeq$300 kW/cm^3).

neon and argon, these show performance peaking at 3–4 Torr HCl.

The low-pump-rate, long-pulse regime is represented by the experiments conducted at Avco,[30] using a pump rate of approximately 80 kW/cm^3 and pulse lengths of 2.5 μs. Both argon (2 atm) and neon (4 atm) buffers were used. Experimental results and model simulations are shown in Figs. 10(a) and 10(b). Although no error bars are presented for the data, the scatter of points between 4 and 5 Torr HCl in

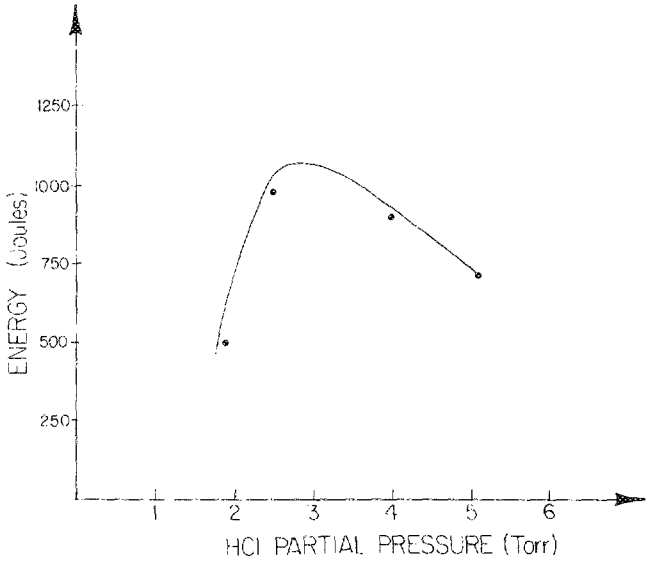

FIG. 9. Data (points) and model simulation (solid line) for laser energy out (joules) vs initial HCl concentration (Torr) in the Thermo Electron Technologies Corporation experiments (Ref. 8). The result of the calculation has been corrected for 10% obscuration of the output windows; differential pumping is not included.

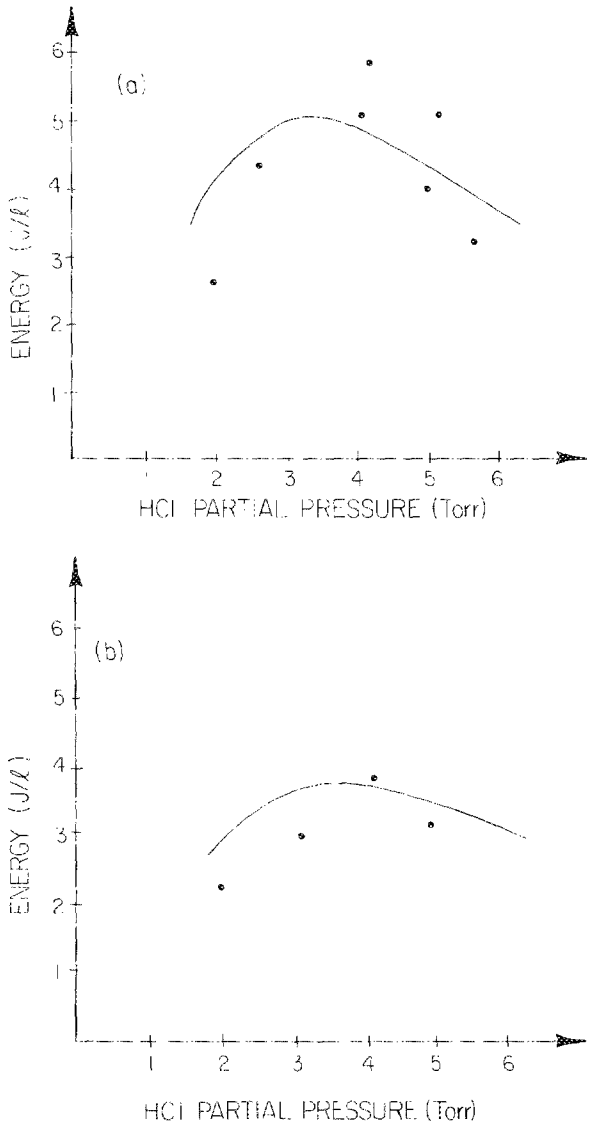

FIG. 10. Data (points) and model simulation (solid line) for laser energy out (joules per liter) vs initial HCl concentration (Torr) in experiments conducted at Avco Everett Research Labs (Ref. 9). The pump power was low ($\simeq$80 kW/cm^3) and the pulse length long (2.5 μs). (a) Argon buffer. (b) Neon buffer.

Fig. 10(a) clearly indicates error bars of at least 1 J/ℓ; all the simulation values lie well within this margin. Some HCl remains present to act as a chlorine donor to the end of the pulse for initial concentrations $\gtrsim$3 Torr. The decrease in performance at high HCl concentrations is due more to quenching of the upper laser level by HCl than to absorption by Cl$_2$. Both model and data demonstrate that XeCl can achieve multimicrosecond pulse lengths at low-power pumping, but with some penalty in efficiency. The best intrinsic efficiencies for these experiments are in the range 2.5%–3%.

The apparent variances in scaling among these results depend variously upon pumping, quenching, and absorption processes, as well as on the particular characteristics of some of the devices themselves. Thus, for instance, the TTC results show a greater sensitivity to HCl concentration than do

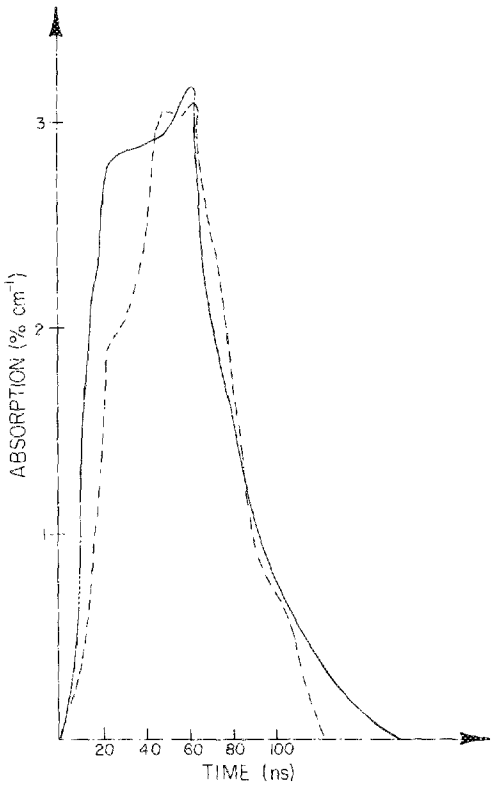

FIG. 11. Data (dashed line) and model simulations (solid line) for total absorption at 312.5 nm (percent per cm) vs time (ns) in the Sandia experiments (Ref. 4) with argon buffer gas.

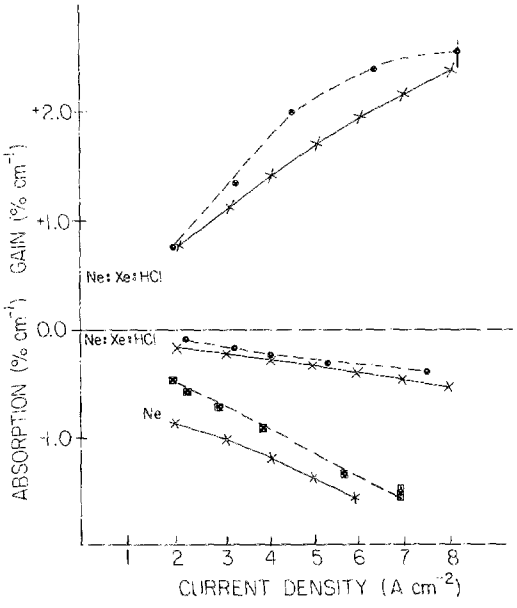

FIG. 12. Measurements (dashed lines and points) and model simulations (solid lines and ×'s) for experiments conducted in XeCl mixtures at the Naval Research Laboratory (Ref. 15). The top graphs show measurement of gain in an Ne:Xe:HCl mixture of concentrations 98.93:1.0:0.67; the center graph shows measurements of integrated absorption in the same mixture; and the bottom graph shows measurements of absorption in pure neon. All measurements are percent per cm, and are plotted against pumping current density (A cm^{-2}).

the Sandia results; this is primarily a result of the 1-m gain length of the former device, which emphasizes integrated absorption. Figure 11 shows the total absorption in the lasing medium for the Sandia experiment, measured at 312.5 nm to eliminate absorption by the XeCl (X) state. The calculation appears to rise slightly faster than the data, but the shape and magnitude are in excellent agreement.

Figure 12 shows experimental results and model simulations of measurements of gain and absorption (top two pairs of curves) in XeCl laser mixtures performed at the Naval Research Laboratory (NRL).[151] These measurements are particularly important to scaling of XeCl performance in the low-to-mid pumping regime (30–300 kW/cm^3), since output flux and extraction efficiency are limited by the ratio of gain to absorption. In the NRL experiments, this ratio remained roughly constant (at a value close to 5) throughout the regime, a consequence of the mutually ionic nature of the dominant process of both pumping and absorption. The excellent agreement of these calculations with data (note the sample error bar in the gain measurement) can be compared with the laser output calculations [Figs. 10(a) and 10(b)] of the noisier Avco data,[30] which is within this pumping regime. Local efficiencies on the order of 3%, achieved in the Avco lasing results, are also predicted from the NRL measurements and simulations. The bottom pair of curves in Fig. 12 show data and simulations from absorption measurements at 308 nm in pure neon. The model's prediction is unacceptably large below about 4 A cm^{-2} because of an overprediction of the Ne_2^+ density. At the lower electron number densities of these pump powers, the variation of the rate constant for dissociative recombination with electron temperature is critical, and the simulation code's energy-balance calculation of T_e is not sufficiently accurate; a fully self-consistent Boltzmann solution would be required to achieve real accuracy here. But this is not necessary, as is manifestly demonstrated by the simulations of laser-mixture absorption in the middle pair of curves; addition of xenon and HCl lowers drastically both the number density of Ne_2^+ and, more important, the sensitivity of the electron chemistry.

Calculations of the relative abundances of major absorbers throughout the laser pulses are shown for both the Avco (neon buffer) and Sandia experiments in Figs. 13(a) and 13(b), respectively. The hard pumping of the Sandia regime produces large numbers of molecular ions (the early peak is an artifact of the shape of the e-beam pulse); as the pump pulse ends, with Cl^- ions still abundant, the rare-gas molecular ions disappear rapidly. By contrast, the much lower pump-power regime of the Avco experiment is initially dominated by Cl^- photodetachment; but as the HCl begins to burn out later in the pulse, this absorption falls steadily. At the same time, the xenon molecular ion density grows because of removal of the neutralization loss mechanism. Early discussions of XeCl kinetics[7,152] suggested that performance using an argon buffer would be significantly worse than using a neon buffer because of the broadband absorption of Ar_2^+. Figures 13(a) and 13(b) show why this turned out to be not true. Although the cross section for Ar_2^+ is roughly twice that for Ne_2^+, total absorption in both low and

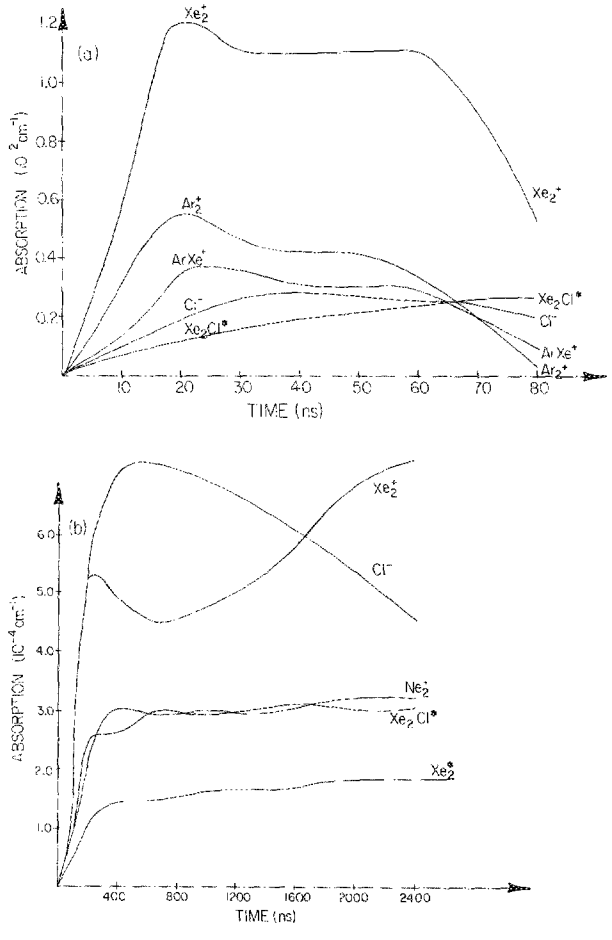

FIG. 13. Model simulations of transient absorptions (cm^{-1}) caused by the principal absorbing species vs laser pulse time (ns). (a) Sandia experiments (Ref. 4). (b) Avco experiments (Ref. 9), neon buffer.

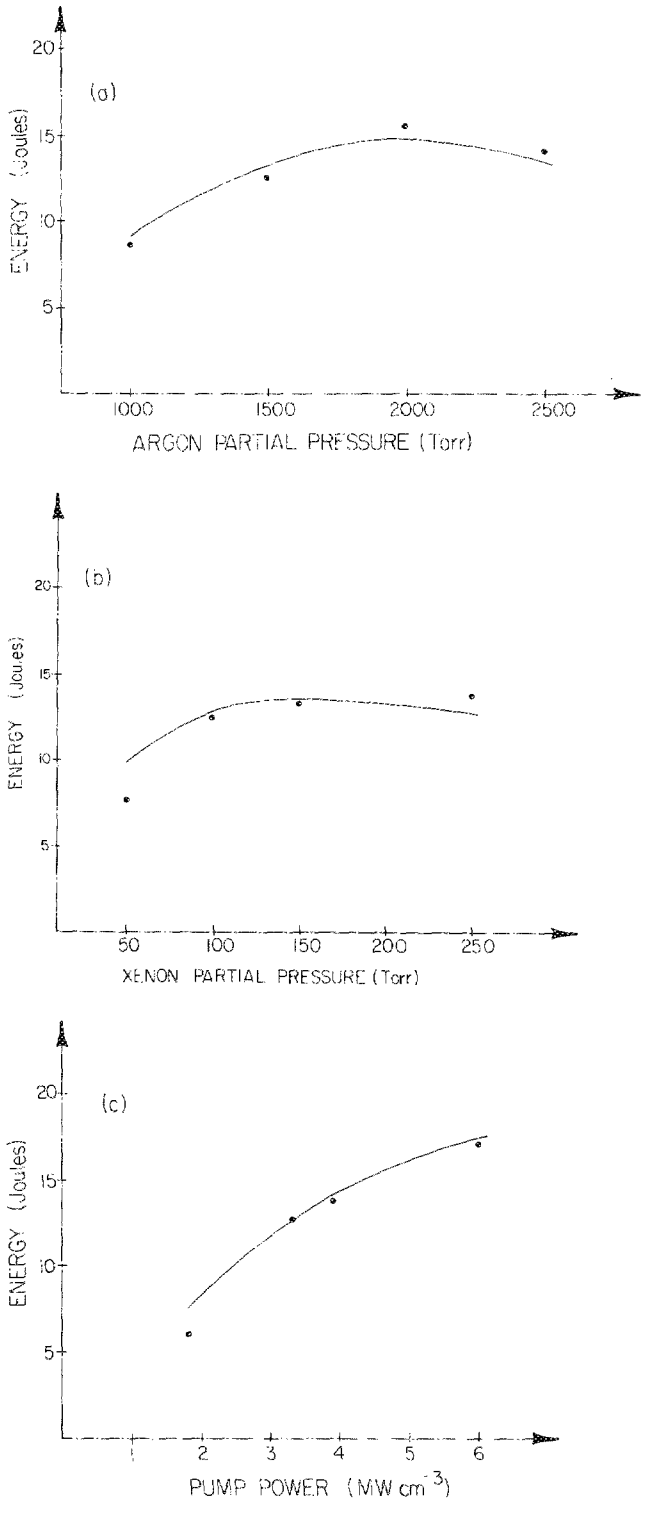

FIG. 14. Data (points) and model simulations (solid lines) for scaling of energy out (joules) in the Sandia experiments (Ref. 4) vs (a) argon pressure (Torr), (b) xenon pressure (Torr), and (c) pump power (MW/cm^3).

high pump regimes is dominated by Xe_2^+ or Cl^-, independent of buffer gas.

Scalings of energy extracted in the Sandia experiment with argon buffer pressure, xenon pressure, and pump power (at constant pressure and mix) are shown in Figs. 14(a)–14(c), respectively. The slight decrease at high argon pressure is caused mostly by three-body quenching; quenching at increased xenon pressure is offset by increased deposition of the *e*-beam energy. Pump power scaling shows significant loss of efficiency as power increases above 3 MW/cm^3 because the production channels are saturated for available chlorine, but ion absorption continues to increase; this could only be slightly ameliorated by increasing initial HCl concentration because of the effectiveness of HCl quenching. Predictions of the model reproduce these scalings precisely.

IV. KINETIC MODEL

The reactions that make up the kinetic model are presented in Table I. Forty-two chemical species (counting electrons and various excited levels of atoms and molecules as separate species) are necessary to specify the reactions.

The electronic manifold of atomic xenon is represented by three excited states, each chosen to represent a group of actual metastable states, as illustrated in Fig. 15. The nominal metastable energies are: Xe*, 8.25 eV; Xe**, 9.5 eV; Xe***, 11.25 eV. These are roughly the energies of the 6*s*, 6*p*, and 4*f* states, respectively. The necessity of including separate states representing the heavily populated first two metastables is reasonably obvious. Performance of the model was also found to require the presence of the third metasta-

TABLE I. Reaction rate model. All rates are in units of $cm^3\ s^{-1}$, except that for reactions involving three chemical species on the left-hand side the units are $cm^6\ s^{-1}$. Rates for emission and absorption processes are given in units of s^{-1} and cm^2, respectively. Parentheses following HCl refer to vibrational excitation levels; absence of parentheses means the process applies to all vibrational levels of HCl. XeCl* denotes the B state (upper laser level); the C, X, and A states are explicitly indicated. ϕ denotes the photon number density. T_e is electron temperature in eV; T_k is electron average energy in eV.

Process		Rate ($cm^3\ s^{-1}$)	Reference	Note
Electron-chlorine reactions				
$e + HCl(0)$	$\rightarrow e + HCl(1)$	1.5×10^{-9}	This work	a
$e + HCl(0)$	$\rightarrow e + HCl(2)$	1.5×10^{-10}	This work	a
$e + HCl(1)$	$\rightarrow e + HCl(2)$	1.5×10^{-9}	This work	a
$e + HCl(0)$	$\rightarrow H + Cl^-$	2.5×10^{-10}	35	
$e + HCl(1)$	$\rightarrow H + Cl^-$	1.1×10^{-8}	36	b
$e + HCl(2)$	$\rightarrow H + Cl^-$	2.0×10^{-7}	36	b
$H + Cl^-$	$\rightarrow HCl + e$	9.6×10^{-10}	37	
$e + Cl_2$	$\rightarrow Cl + Cl^-$	1.0×10^{-10}	38	
Electron-rare gas reactions				
$e + Xe$	$\rightarrow e + Xe^*$	$1.2\times10^{-8}\,T_k^{0.72}\exp(-8.36/T_k)$	39,150	c
$e + Xe$	$\rightarrow e + Xe^{**}$	$2.8\times10^{-8}\,T_k^{0.725}\exp(-8.73/T_k)$	39,150	c
$e + Xe^*$	$\rightarrow e + Xe^{**}$	$10^{(-4.28/T_k^{0.36}-1.81/T_k^{0.51})}$	40	
$e + Xe^*$	$\rightarrow e + Xe$	$1.2\times10^{-8}\,T_k^{0.72}\exp(-8.36/T_k)$	39,150	c
$e + Xe^{**}$	$\rightarrow e + Xe$	$2.8\times10^{-8}\,T_k^{0.75}\exp(-9.73/T_k)$	39,150	c
$e + Xe^{**}$	$\rightarrow e + Xe^*$	$10^{(-7.07+0.1T_k)}$	40	
$e + Xe$	$\rightarrow 2e + Xe^+$	$3.47\times10^{-8}\,T_k^{0.72}\exp(-12.13/T_k)$	39,144	c
$e + Xe^*$	$\rightarrow 2e + Xe^+$	$7.85\times10^{-8}\,T_k^{0.71}\exp(-3.77/T_k)$	39,145,146	c
$e + Xe^{**}$	$\rightarrow 2e + Xe^+$	$2.15\times10^{-7}\,T_k^{0.71}\exp(-2.4/T_k)$	39,145,146	c
$e + Xe_2^*$	$\rightarrow 2e + Xe_2^+$	$9.75\times10^{-8}\,T_k^{0.705}\exp(-3.4/T_k)$	39,145,146	c
$e + Xe_2^+$	$\rightarrow Xe + Xe^{**}$	$2.0\times10^{-7}/T_k^{0.5}$	42,43	
$e + Xe^*$	$\rightarrow e + Xe^{***}$	$(0.02)10^{(-4.88/T_k^{0.36}-1.81/T_k^{0.51})}$	40	
$e + Xe^{**}$	$\rightarrow e + Xe^{***}$	$10^{(-4.88/T_k^{0.36}-1.81/T_k^{0.51})}$	40	
$e + Xe^{***}$	$\rightarrow e + Xe^{**}$	$10^{(-7.07+0.1T_k)}$	40	
$e + Xe^{***}$	$\rightarrow e + Xe^*$	$(0.02)10^{(-4.88/T_k^{0.36}-1.81/T_k^{0.51})}$	40	
$e + Xe^{***}$	$\rightarrow 2e + Xe^+$	$2.15\times10^{-7}\,T_k^{0.71}\exp(-2.4/T_k)$	39,145,146	c
$e + Ar$	$\rightarrow e + Ar^*$	$1.0\times10^{-11}\,T_e^{0.75}$	41,139,140,141	d
$e + Ar$	$\rightarrow e + Ar^{**}$	$5.0\times10^{-12}\,T_e^{0.5}$	41,139,140,141	d
$e + Ar^*$	$\rightarrow e + Ar^{**}$	$2.0\times10^{-7}\,T_e$	41,142,147	d
$e + Ar^*$	$\rightarrow e + Ar$	$1.0\times10^{-11}\,T_e^{0.75}$	41,139,140,141	d
$e + Ar^{**}$	$\rightarrow e + Ar$	$5.0\times10^{-12}\,T_e^{0.50}$	41,139,140,141	d
$e + Ar^{**}$	$\rightarrow e + Ar^*$	$2.0\times10^{-7}\,T_e$	41,142,147	d
$e + Ar$	$\rightarrow 2e + Ar^+$	$4.0\times10^{-12}\,T_e^{0.5}$	41,143,144,148	d
$e + Ar^*$	$\rightarrow 2e + Ar^+$	$1.0\times10^{-10}\,T_e^3$	41,145,146	d
$e + Ar^{**}$	$\rightarrow 2e + Ar^+$	$4.0\times10^{-9}\,T_e^2$	41,145,146	d
$e + Ar_2^*$	$\rightarrow 2e + Ar_2^+$	$4.0\times10^{-10}\,T_e^3$	41,145,146	d
$e + Ar_2^+$	$\rightarrow Ar + Ar^{**}$	$8.0\times10^{-8}\,T_e^{0.5}$	42	
$e + ArXe^*$	$\rightarrow ArXe^+ + 2e$	$4.0\times10^{-10}\,T_e^3$	41,145,146	d
$e + Ne$	$\rightarrow e + Ne^*$	$5.05\times10^{-9}\,T_k^{1.69}\exp(-16.6/T_k)$	39,149,139,141	c
$e + Ne$	$\rightarrow e + Ne^{**}$	$5.85\times10^{-10}\,T_k^{0.48}\exp(-18.5/T_k)$	39,139,141	c
$e + Ne^*$	$\rightarrow e + Ne^{**}$	$4.36\times10^{-7}\,T_k^{0.32}\exp(-1.90/T_k)$	39,142	c
$e + Ne^*$	$\rightarrow e + Ne$	$5.05\times10^{-9}\,T_k^{1.69}\exp(-16.6/T_k)$	39,149,139,141	c
$e + Ne^{**}$	$\rightarrow e + Ne$	$5.85\times10^{-10}\,T_k^{0.48}\exp(-18.5/T_k)$	39,139,141	c
$e + Ne^{**}$	$\rightarrow e + Ne^*$	$4.36\times10^{-7}\,T_k^{0.32}\exp(-1.90/T_k)$	39,142	c
$e + Ne$	$\rightarrow 2e + Ne^+$	$1.65\times10^{-9}\,T_k^{0.724}\exp(-21.6/T_k)$	39,144,148	c
$e + Ne^*$	$\rightarrow 2e + Ne^+$	$4.1\times10^{-8}\,T_k^{0.74}\exp(-5.0/T_k)$	39,145,146	c
$e + Ne^{**}$	$\rightarrow 2e + Ne^+$	$1.28\times10^{-7}\,T_k^{0.60}\exp(-3.1/T_k)$	39,145,146	c
$e + Ne_2^*$	$\rightarrow 2e + Ne_2^+$	$6.5\times10^{-8}\,T_k^{0.68}\exp(-4.3/T_k)$	39,145,146	c
$e + Ne_2^+$	$\rightarrow Ne + Ne^{**}$	$3.5\times10^{-8}\,T_k^{0.5}$	42,44	
$e + NeXe^*$	$\rightarrow NeXe^+ + 2e$	$8.0\times10^{-8}\,T_k^{0.71}\exp(-3.60/T_k)$	39,145,146	c
$e + NeXe^+$	$\rightarrow Xe^{**} + Ne$	$8.0\times10^{-8}\,T_k^{0.5}$	42,43,44	e
$e + ArXe^+$	$\rightarrow Xe^{**} + Ar$	$1.0\times10^{-7}\,T_k^{0.5}$	42,43,44	e
Penning ionization				
$Xe^* + Xe^*$	$\rightarrow Xe^+ + Xe + e$	5.0×10^{-10}	47,95	
$Xe_2^* + Xe_2^*$	$\rightarrow Xe_2^+ + 2Xe + e$	5.0×10^{-10}	47,125,95	

TABLE I. (*Continued*).

Process		Rate ($cm^3 s^{-1}$)	Reference	Note
$Xe^{***} + Xe$	$\rightarrow Xe_2^+ + e$	2.0×10^{-10}	48	
$Ar^{**} + Xe$	$\rightarrow Ar + Xe^+ + e$	2.0×10^{-10}	48	
$Ar^* + Ar^*$	$\rightarrow Ar^+ + Ar + e$	5.0×10^{-10}	50,51	f
$Ar_2^* + Ar_2^*$	$\rightarrow Ar_2^+ + 2Ar + e$	5.0×10^{-10}	50,51	f
$Ne^* + Xe$	$\rightarrow NeXe^+ + e$	2.3×10^{-11}	45,46,72,116	
$Ne_2^* + Xe$	$\rightarrow NeXe^+ + Ne + e$	2.3×10^{-11}	46,45	
$Ne^* + Xe$	$\rightarrow Xe^+ + Ne + e$	7.5×10^{-12}	45,46,49,72,116	
$Ne_2^* + Xe$	$\rightarrow 2Ne + Xe^+ + e$	7.5×10^{-11}	46,45,49	
$Ne_2^* + Ne_2^*$	$\rightarrow Ne_2^+ + 2Ne + e$	5.0×10^{-10}	50,51	f
$Ne^* + Ne^*$	$\rightarrow Ne^+ + Ne + e$	5.0×10^{-10}	50,51	f
Dimer ion formation				
$Xe^+ + 2Xe$	$\rightarrow Xe_2^+ + Xe$	2.5×10^{-31}	52,53,124	
$Xe^+ + Xe + Ar$	$\rightarrow Xe_2^+ + Ar$	2.0×10^{-31}	58,64	
$Xe^+ + Xe + Ne$	$\rightarrow Xe_2^+ + Ne$	1.5×10^{-31}	46,58	
$Xe^+ + 2Ar$	$\rightarrow ArXe^+ + Ar$	1.0×10^{-31}	61,62,115	
$Ar^+ + Xe + Ar$	$\rightarrow ArXe^+ + Ar$	1.0×10^{-31}	61	
$Ar^+ + 2Ar$	$\rightarrow Ar_2^+ + Ar$	2.5×10^{-31}	54,55,80	
$Xe^+ + 2Ne$	$\rightarrow NeXe^+ + Ne$	1.0×10^{-31}	57,58	
$Ne^+ + Xe + Ne$	$\rightarrow NeXe^+ + Ne$	1.0×10^{-31}	57	
$Ne^+ + 2Ne$	$\rightarrow Ne_2^+ + Ne$	4.4×10^{-32}	56	
Charge exchange reactions				
$Ar_2^+ + Xe + Ar$	$\rightarrow Xe^+ + 3Ar$	1.0×10^{-29}	63,64	g
$ArXe^+ + Xe$	$\rightarrow Xe^+ + Ar + Xe$	5.0×10^{-10}	65	h
$ArXe^+ + Xe$	$\rightarrow Xe_2^+ + Ar$	1.0×10^{-11}	65,115	
$Ne_2^+ + Xe + Ne$	$\rightarrow Xe^+ + 3Ne$	4.0×10^{-30}	63	
$NeXe^+ + Xe$	$\rightarrow Xe^+ + Ne + Xe$	5.0×10^{-10}	65	h
$NeXe^+ + Xe$	$\rightarrow Xe_2^+ + Ne$	5.0×10^{-12}	65	h
$Xe + Cl^+$	$\rightarrow Xe^+ + Cl$	1.0×10^{-12}	39	i
$Xe + HCl^+$	$\rightarrow Xe^+ + HCl$	3.4×10^{-10}	59,112	
$Ar^+ + Xe$	$\rightarrow Xe^+ + Ar$	4.3×10^{-13}	60	
$Ne^+ + Xe$	$\rightarrow Xe^+ + Ne$	4.3×10^{-17}	60	
Neutralization reactions				
$Xe^+ + Cl^-$	$\rightarrow XeCl^*$	$5.0\times10^{-7} P$	66,68	j
$Xe_2^+ + Cl^-$	$\rightarrow XeCl^* + Xe$	Same	66,68	j
$ArXe^+ + Cl^-$	$\rightarrow XeCl^* + Ar$	Same	58,68	j
$Ar^+ + Cl^-$	$\rightarrow ArCl^*$	Same	68	j
$Ar_2^+ + Cl^-$	$\rightarrow ArCl^* + Ar$	Same	68	j
$NeXe^+ + Cl^-$	$\rightarrow XeCl^* + Ne$	Same	58,68	j
$Ne_2^+ + Cl^-$	$\rightarrow Cl^* + 2Ne$	Same	66,67,68	j,k
$Ne^+ + Cl^-$	$\rightarrow Cl^* + Ne$	Same	66,67,68	j
$Cl^+ + Cl^-$	$\rightarrow Cl_2^*$	2.0×10^{-6}	68	
Neutral kinetics				
$Xe^* + HCl(1)$	$\rightarrow XeCl^* + H$	2.0×10^{-10}	69	
$Xe^{**} + HCl(1)$	$\rightarrow XeCl^* + H$	5.6×10^{-10}	70,81	
$Xe^{**} + HCl(0)$	$\rightarrow XeCl^* + H$	5.6×10^{-10}	70,81	
$Xe + Cl_2^*$	$\rightarrow XeCl^* + Cl$	5.0×10^{-10}	71	
$Xe^{***} + HCl(0)$	$\rightarrow XeCl^* + H$	5.6×10^{-10}	70,81	
$Xe^{***} + HCl(1)$	$\rightarrow XeCl^* + H$	5.6×10^{-10}	70,81	
$Xe^* + HCl(2)$	$\rightarrow XeCl^* + H$	2.0×10^{-10}	69	
$Xe^{**} + HCl(2)$	$\rightarrow XeCl^* + H$	5.6×10^{-10}	70,81	
$Xe^{***} + HCl(2)$	$\rightarrow XeCl^* + H$	5.6×10^{-10}	70,81	
$Ar^* + 2Ar$	$\rightarrow Ar_2^* + Ar$	1.1×10^{-32}	77,78,79,113	
$Ar^{**} + Ar$	$\rightarrow Ar^* + Ar$	1.0×10^{-10}	84	
$Xe^* + 2Ar$	$\rightarrow ArXe^* + Ar$	1.0×10^{-33}	73	
$Xe^{**} + Ar$	$\rightarrow Xe^* + Ar$	1.0×10^{-11}	84	
$Xe^* + Xe + Ar$	$\rightarrow Xe_2^* + Ar$	2.3×10^{-32}	74	

TABLE I. (*Continued*).

Process		Rate ($cm^3 s^{-1}$)	Reference	Note
$ArXe^* + Xe$	$\rightarrow Xe_2^* + Ar$	1.0×10^{-10}	50	
$Ar^* + Xe$	$\rightarrow Xe^{**} + Ar$	2.1×10^{-10}	82,83,113	
$Ar^* + Xe$	$\rightarrow ArXe^*$	5.0×10^{-11}	84	l
$Ar_2^* + Xe$	$\rightarrow Xe^* + 2Ar$	2.4×10^{-10}	50,85,113,114	
$Ar_2^* + Xe$	$\rightarrow ArXe^* + Ar$	5.0×10^{-11}	84	l
$Xe^{***} + Ar$	$\rightarrow Xe^{**} + Ar$	1.0×10^{-11}	84	
$Ne^* + 2Ne$	$\rightarrow Ne_2^* + Ne$	4.0×10^{-34}	72	
$Ne^{**} + Ne$	$\rightarrow Ne^* + Ne$	7.0×10^{-11}	86	
$Xe^* + 2Ne$	$\rightarrow NeXe^* + Ne$	5.0×10^{-34}	57,39	m
$Xe^{**} + Ne$	$\rightarrow Xe^* + Ne$	1.0×10^{-11}	86	
$Xe^* + 2Xe$	$\rightarrow Xe_2^* + Xe$	5.0×10^{-32}	74,75,76	
$Cl^* + HCl$	$\rightarrow Cl_2^* + H$	5.0×10^{-10}	estimated	n
$Cl + Cl + Xe$	$\rightarrow Cl_2 + Xe$	2.5×10^{-33}	127	
$Xe^* + Xe + Ne$	$\rightarrow Xe_2^* + Ne$	1.6×10^{-32}	72	
$NeXe^* + Xe$	$\rightarrow Xe_2^* + Ne$	1.0×10^{-10}	57,39	
$Xe^{***} + Ne$	$\rightarrow Xe^{**} + Ne$	1.0×10^{-11}	86	
Displacement channel				
$Ar^* + HCl(0)$	$\rightarrow ArCl^* + H$	5.6×10^{-10}	81,68	
$Ar^{**} + HCl(0)$	$\rightarrow ArCl^* + H$	5.6×10^{-10}	81,68	
$Ar^* + HCl(1)$	$\rightarrow ArCl^* + H$	5.6×10^{-10}	81,68	
$Ar^{**} + HCl(1)$	$\rightarrow ArCl^* + H$	5.6×10^{-10}	81,68	
$Ar^* + HCl(2)$	$\rightarrow ArCl^* + H$	5.6×10^{-10}	81,68	
$Ar^{**} + HCl(2)$	$\rightarrow ArCl^* + H$	5.6×10^{-10}	81,68	
$ArCl^* + Xe$	$\rightarrow XeCl^* + Ar$	1.5×10^{-10}	87,88	
Quenching reactions				
$XeCl^* + Ar$	$\rightarrow Xe + Cl + Ar$	2.0×10^{-13}	89	
$XeCl^* + 2Ar$	$\rightarrow Xe + Cl + Ar$	3.0×10^{-33}	89	
$XeCl^* + Ne$	$\rightarrow Xe + Cl + Ne$	3.3×10^{-13}	90	
$XeCl^* + 2Ne$	$\rightarrow Xe + Cl + 2Ne$	1.0×10^{-33}	91	
$XeCl^* + e$	$\rightarrow Xe + Cl + e$	2.0×10^{-8}	92, this model	o
$XeCl^* + HCl$	$\rightarrow Xe + HCl + Cl$	8.0×10^{-10}	93,94,104	p
$XeCl^* + Xe + M$	$\rightarrow Xe_2Cl^* + M$	5.0×10^{-31}	100,123	q
$Xe_2Cl^* + HCl$	$\rightarrow 2Xe + HCl + Cl$	8.0×10^{-10}	100	
$XeCl^* + Cl$	$\rightarrow Xe + 2Cl$	8.0×10^{-10}	100	
$XeCl^*(C) + Xe + M$	$\rightarrow Xe_2Cl^* + M$	5.0×10^{-31}	100,123	
$XeCl^*(C) + HCl$	$\rightarrow Xe + HCl + Cl$	8.0×10^{-10}	93,94,104	p
$ArCl^* + e$	$\rightarrow Ar + Cl + e$	2.0×10^{-8}	92, this model	o
$Ar_2^* + e$	$\rightarrow 2Ar + e$	1.0×10^{-9}	95	
$ArXe^* + e$	$\rightarrow Ar + Xe + e$	1.0×10^{-9}	95	
$Ne_2^* + e$	$\rightarrow 2Ne + e$	1.0×10^{-8}	95	
$NeXe^* + e$	$\rightarrow Ne + Xe + e$	1.0×10^{-9}	95	
$Xe_2Cl^* + e$	$\rightarrow 2Xe + Cl + e$	2.0×10^{-8}	92, this model	o
$Xe_2^* + e$	$\rightarrow 2Xe + e$	1.0×10^{-9}	95	
$Cl^* + e$	$\rightarrow Cl + e$	2.0×10^{-8}	estimated	r
$Cl_2^* + e$	$\rightarrow Cl_2 + e$	2.0×10^{-8}	estimated	r
$Xe^* + HCl$	$\rightarrow Xe + H + Cl$	5.6×10^{-10}	96	p
$Xe_2Cl^* + Xe$	$\rightarrow 3Xe + Cl$	5.0×10^{-13}	97,100	
$Xe_2Cl^* + M$	$\rightarrow 2Xe + Cl + M$	3.0×10^{-14}	97	
$Xe_2Cl^* + Cl_2$	$\rightarrow 2Xe + Cl + Cl_2$	4.0×10^{-10}	127	
$HCl(0) + e$	$\rightarrow H + Cl + e$	7.0×10^{-12}	128	s
$HCl(1) + e$	$\rightarrow H + Cl + e$	1.2×10^{-11}	128	s
$HCl(1) + HCl(0)$	$\rightarrow 2HCl(0)$	1.0×10^{-11}	130	
$HCl(1) + H$	$\rightarrow HCl(0) + H$	7.0×10^{-12}	130	
$HCl(1) + Cl$	$\rightarrow HCl(0) + Cl$	7.0×10^{-12}	130	
$XeCl^* + Xe$	$\rightarrow 2Xe + Cl$	2.3×10^{-11}	104,106	
$XeCl^*(C) + Xe$	$\rightarrow 2Xe + Cl$	2.3×10^{-11}	104,106	
XeCl *C* and *X* state reactions				
$XeCl^* + e$	$\rightarrow XeCl^*(C) + e$	2.0×10^{-8}	92, this model	t
$XeCl^*(C) + e$	$\rightarrow XeCl^* + e$	2.0×10^{-8}	92, this model	t

TABLE I. (*Continued*).

Process		Rate ($cm^3 s^{-1}$)	Reference	Note
$XeCl^* + M$	$\rightarrow XeCl^*(C) + M$	8.0×10^{-10}	104	
$XeCl^*(C) + M$	$\rightarrow XeCl^* + M$	8.0×10^{-10}	104	
$XeCl(X) + M$	$\rightarrow Xe + Cl + M$	8.0×10^{-12}	59,107	u
$Xe + Cl + M$	$\rightarrow XeCl(X) + M$	1.2×10^{-33}	108	
$XeCl(X) + HCl$	$\rightarrow Xe + Cl + HCl$	2.2×10^{-11}	107	
$XeCl(X) + e$	$\rightarrow XeCl(A) + e$	2.0×10^{-8}	92, this model	v
Emission		$1/\tau\ (s^{-1})$		
$XeCl^*$	$\rightarrow XeCl(X) + \phi$	6.0×10^{7}	90,104,105	
$XeCl^*(C)$	$\rightarrow XeCl(A) + \phi$	8.3×10^{6}	104,105	v
$XeCl^* + \phi$	$\rightarrow XeCl(X) + 2\phi$	$4.2\times10^{-16}\ cm^2$	This work	w
Xe_2Cl^*	$\rightarrow 2Xe + Cl + \phi$	7.4×10^{6}	100	
Xe_2^*	$\rightarrow 2Xe + \phi$	6.0×10^{7}	52,102	bb
Xe^{**}	$\rightarrow Xe + \phi$	1.5×10^{7}	52,84	y
Cl_2^*	$\rightarrow Cl_2 + \phi$	5.0×10^{7}	71	z
Cl^*	$\rightarrow Cl + \phi$	1.0×10^{7}	71	aa
Xe^{***}	$\rightarrow Xe^{**} + \phi$	1.5×10^{7}	52,84	y
$ArCl^*$	$\rightarrow Ar + Cl + \phi$	2.4×10^{8}	98	
Ar_2^*	$\rightarrow 2Ar + \phi$	6.0×10^{7}	102	bb
$ArXe^*$	$\rightarrow Ar + Xe + \phi$	5.0×10^{7}	84	x
Ne_2^*	$\rightarrow 2Ne + \phi$	7.5×10^{7}	52	
$NeXe^*$	$\rightarrow Ne + Xe + \phi$	5.0×10^{7}	71	z
Ne^{**}	$\rightarrow Ne + \phi$	6.0×10^{7}	52	
Absorption		$\sigma\ (cm^2)$		
$XeCl(X) + \phi$	$\rightarrow XeCl^*$	1.4×10^{-16}	This work	cc
$Xe_2Cl^* + \phi$	$\rightarrow XeCl^* + Xe$	2.4×10^{-17}	126	
$Cl^- + \phi$	$\rightarrow Cl + e$	1.2×10^{-17}	101	
$Xe^{***} + \phi$	$\rightarrow Xe^+ + e$	1.8×10^{-18}	117	ff
$Xe^{**} + \phi$	$\rightarrow Xe^+ + e$	5.0×10^{-18}	117	
$Xe^* + \phi$	$\rightarrow Xe^+ + e$	6.0×10^{-20}	119	
$Xe_2^+ + \phi$	$\rightarrow Xe^+ + Xe$	2.5×10^{-17}	109,110	
$Xe_2^* + \phi$	$\rightarrow Xe_2^+ + e$	1.4×10^{-17}	52,67	
$Cl_2 + \phi$	$\rightarrow Cl_2^*$	1.7×10^{-19}	120	
$Cl^* + \phi$	$\rightarrow Cl^+ + e$	5.0×10^{-18}	52	ee
$Ar^{**} + \phi$	$\rightarrow Ar^+ + e$	3.5×10^{-18}	117	
$Ar_2^* + \phi$	$\rightarrow Ar_2^+ + e$	1.4×10^{-17}	84,118,52	
$ArXe^* + \phi$	$\rightarrow ArXe^+ + e$	1.5×10^{-17}	41,121,122	dd
$ArXe^+ + \phi$	$\rightarrow Ar + Xe^+$	1.5×10^{-17}	41,121,122	dd
$Ar_2^+ + \phi$	$\rightarrow Ar^+ + Ar$	3.5×10^{-17}	103,109,110	
$Ne^{**} + \phi$	$\rightarrow Ne^+ + e$	2.3×10^{-18}	39,117	
$NeXe^* + \phi$	$\rightarrow NeXe^+ + e$	1.0×10^{-19}	39	gg
$NeXe^+ + \phi$	$\rightarrow Xe^+ + Ne$	1.0×10^{-19}	39	gg
$Ne_2^+ + \phi$	$\rightarrow Ne^+ + Ne$	1.9×10^{-17}	111	
$Ne_2^* + \phi$	$\rightarrow Ne_2^+ + e$	1.0×10^{-17}	52	
$Xe + Cl + \phi$	$\rightarrow XeCl^*$	1.0×10^{-37}	104	hh

[a] Inferred from modeling and analysis of the experiment of Center *et al.* (Ref. 34). These values incorporate deexcitation losses by superelastic collisions. See discussion of HCl excitation in Sec. V.

[b] Cross sections measured by Allan and Wong (Ref. 36), integrated over Maxwellian electron distributions. In the range 0.5–3 eV the resulting rates are so slowly varying as a function of T_e that they can be represented by these single values.

[c] Rate formula taken from Ref. 39, checked by integration over successive Maxwellian distributions of cross-section data from other listed reference(s).

[d] Rate formula fit to successive integrations over Maxwellian distributions of cross-section data from listed reference(s), agrees roughly with curves in Ref. 41.

[e] Estimated by the authors using analogy with Refs. 42, 43, and 44.

[f] Gas-kinetic saturated rate, analogous to measurement in krypton in Ref. 51.

[g] Analogy with Ref. 63.

[h] Analogy and extrapolation from Ref. 65.

[i] The rate quoted in Ref. 39 is given as a guess made by M. Kraus at the 32nd Annual Gaseous Electronics Conference, Pittsburgh, PA, Oct., 1979. The concentration of Cl^+ generally remains small enough that the accuracy of this guess is not important.

[j] $P \equiv \Sigma$ pressures of Xe, Ar, and Ne, in atmospheres.

[k] Analogy to Ref. 67.

[l] Guessed in Ref. 84.

TABLE I. (*Continued*).

[m] Reference 39 contains a private communication source for this rate.
[n] Estimated as a saturated gas kinetic rate by the authors based upon energetics and analogy with Ref. 81.
[o] See discussion of electron quenching in Sec. V.
[p] Rate identical for all vibrational states of HCl. Roughly twice as large as measured by Ref. 104.
[q] M ≡ any heavy body. See discussion on xenon quenching in Sec. V.
[r] Estimated by the authors during private communication discussions of electron quenching processes with D. L. Huestis, SRI International.
[s] Electron-impact dissociation cross sections from Ref. 128 integrated over 2-eV Maxwellian electron distribution. An electron energy of at least 10 eV would be required to make this process competitive with dissociative attachment.
[t] Electron mixing rates for *B* and *C* states estimated by analogy with electron quenching rates for the same states. See Sec. V.
[u] See discussion of ground-state dissociation in Sec. V.
[v] XeCl(*A*) state is dissociative, resulting in Xe + Cl.
[w] Stimulated emission cross section discussed in Sec. II.
[x] Estimated in Ref. 84.
[y] Estimated in Ref. 84 by analogy with Ref. 31.
[z] Estimated by D. L. Huestis, SRI International in analogy with Ref. 46.
[aa] Assumed upper limit for quartet-to-doublet radiative rate.
[bb] Average of singlet and triplet lifetimes, weighted by state populations.
[cc] Cross-section discussed in Sec. II.
[dd] Estimated in Ref. 41 by analogy with $ArKr^+$ from Ref. 121, and from analysis in Ref. 122.
[ee] Estimated by analogy with excited rare gas molecule photoionization cross-sections in Ref. 52.
[ff] Estimated by analogy with results in Ref. 117.
[gg] Guessed by the authors of Ref. 39, based partly upon their modeling. Number densities of these absorbers are low enough that the model is not sensitive to order-of-magnitude variation of this cross section.
[hh] Estimated from calculations and modeling; see Sec. V.

ble about 1 eV from the ionization threshold in order to follow the ionic species accurately, and to model laser absorption by photoionization. However, a fourth metastable, to provide a finer structure within the bands represented by either Xe** or Xe***, is not important to the accuracy of the model, especially compared to uncertainties in the rates of certain other processes discussed in Sec. V.

The model follows two vibrationally excited states of HCl, in addition to a ground state. Since the dissociative attachment rate of HCl ($V = 2$) is more than an order of magnitude greater than the electron-impact excitation rate to HCl ($V = 3$), tracking higher vibrational levels would be superfluous. Effective HCl attachment rates have been a subject of considerable interest and controversy in modeling XeCl, and are also discussed in Sec. V.

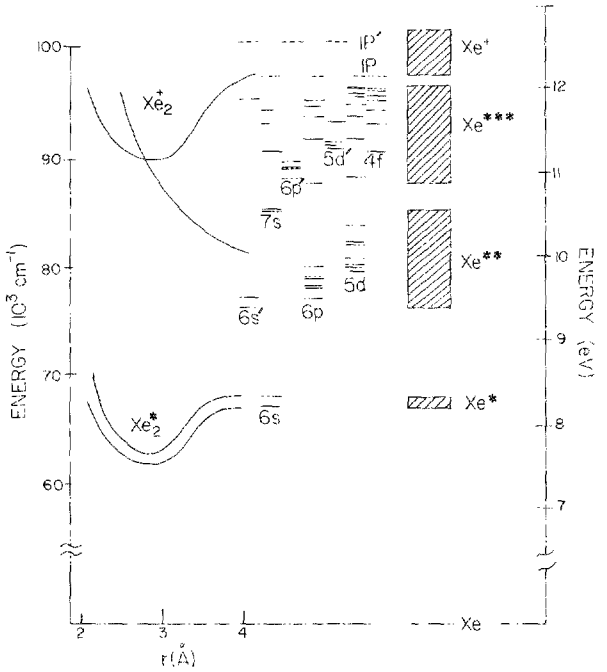

FIG. 15. Xenon metastable manifold, showing how the kinetic model agglomerates excited metastable states into Xe*, Xe**, and Xe***.

Deposition of energy in the gas by *e* beams follows in general the formulation of Lorents[31] to describe species formation. That is, beam electrons produce both ions and excited metastables of the rare-gas atoms, with a prescribed fraction of the beam energy going into scattered secondary electrons. The general deposition of energy can than be compared to calculations using Monte Carlo codes,[32] and the comparison is excellent. Deposition fractions used for argon (26.05 eV/ion pair total) are: 15.76 eV to ionization; 3.29 to excitation; 7.0 eV to electrons. Similar numbers for neon (41 eV/ion pair) are 21.6, 5.20, and 14.2 eV, respectively, and for xenon (21.26 eV/ion pair) 12.2, 2.06, and 7.0 eV, respectively. Berger–Seltzer cross sections[33] at appropriate electron energy are used, multiplied by a factor of 2.8 to account for three-dimensional (3D) effects.

The secondary electron temperature is calculated by balancing the energy flow into and out of the electron gas from deposition of the *e*-beam energy and from the various inelastic scattering processes, such as recombination and attachment. Rates for electron kinetic processes are then calculated using this temperature from fits to convolutions of the relevant cross sections over Maxwellian electron distributions at various temperatures. The electron distribution in such an *e*-beam-pumped gas with an attaching molecule present is certainly not Maxwellian, but the deviations appear not to be important for the purposes of this kinetic modeling. Electron impact ionization and excitation of the rare gases depend only on the high-energy tail of the distribution, and in any case these remain minute compared to the contributions of the electron beam. For processes that do depend upon lower-energy electrons—such as dissociative attach-

ment and dissociative recombination—we have checked the validity of the electron temperature modeling process two ways. First, Boltzmann code calculations producing non-Maxwellian profiles have been used to recalculate rates of critical processes at representative electron temperatures (e.g., 1.8 eV); second, arbitrary analytic distribution functions, chosen as limits of the shapes produced by the Boltzmann calculations, have been separately convolved to calculate the key rates. In pure rare gases at very low pump rates (such as the low end of the NRL experiment discussed above), the electron temperature model may not be sufficiently accurate. But for laser gas mixtures, and for all mixtures at pump rates above about 75 kW/cm^3, neither of the comparison procedures produced kinetics results significantly different from those of the simpler electron temperature model. In Table I, analytic expressions for kinetic rates as functions of electron temperature or energy are given in place of single rates for the electron processes. The expressions are obtained from fits to Boltzmann calculations, as described above. Some of the expressions have been taken from similar fits given in Ref. 39, but these as well were checked by the present authors using a Boltzmann code and the cross sections referenced in Table I.

The C state of XeCl* and its associated processes are carried explicitly in the model. B-to-C state mixing, principally by heavy body collisions, mixes the two states very rapidly; the ratio of B-to-C state population densities typically varies from 1.5 to 3.0, depending on pumping conditions, gas mix, and time elapsed in the pump pulse.

The simulations presented here are accomplished by simultaneous solution of the rate equations associated with the reactions in Table I in a Fortran computer code. The general design of this code, including the integration methods, Boltzmann solution, and Rigrod extraction model, are described in an earlier paper.[129]

V. KINETICS ISSUES

The major kinetics issue in xenon chloride is in fact a tightly connected complex of issues that must find a common solution. In general, these issues relate the electrons, the halogen donor (HCl), and the processes through which those species directly influence pumping and quenching of XeCl. The extent and difficulty of the interactions is illustrated by the conflicting implications of a few of the key experiments. Long-pulse lasing experiments,[9] together with moderate pulse-length experiments,[8] suggest that HCl burns up at a steady, gradual pace during the laser pulse. A series of kinetics experiments[12] measured electron densities for mid-length pulses (of roughly the excitation levels of Ref. 8) and showed sudden jumps in mid pulse for low initial HCl pressures; these results suggest that HCl burns up rapidly. Attachment rates for vibrationally excited HCl are known to be high,[26] and various measurements of the excitation cross sections for HCl by secondary electrons[131] suggest that, for secondary electron temperatures in the 1–2 eV range, the excited HCl could be a large fraction (on the order of 30%) of the initial concentration. On the other hand, direct experiments[132] measured the excited HCl concentration as never exceeding 8%. Finally, fluorescence measurements of XeCl(B) (Ref. 12), suggested that at low HCl concentrations electron quenching dominates over HCl quenching, but strong electron quenching is inconsistent with the combination of high electron densities and laser performance data. In sum, electrons do and do not excite HCl rapidly, do and do not quench XeCl* rapidly, and do and do not deplete HCl rapidly.

The starting place for the current model in this controversy is the experiment of Center *et al.*[132] on excited HCl concentrations. Previous models of XeCl kinetics have used excitation rates for $\Delta V = 1$ transitions in HCl on the order of 2.5×10^{-8} cm^3 s^{-1} for electrons in the temperature range 1–2 eV. Integration of experimentally derived cross sections[131] over a 2-eV Maxwellian yields a value of about 6.0×10^{-9} cm^3 s^{-1}. Using either of these values produces an excited fraction of HCl in the 30% range, as suggested above .The measurements of Center *et al.*, Fig. 16, show a variation in excited HCl fraction as a function of pump power for two different initial HCl concentrations; this excited fraction varies between about 1% and about 8%. Since the value of the excitation rate constant calculated from the cross-section data does not include superelastic deexcitation, it is clear that an effective overall excitation rate would be somewhat lower. The value of 1.5×10^{-9} cm^3 s^{-1} used in the present model was chosen because it provides an excellent fit (Fig. 16) to the Center *et al.* results, and is quantitatively a balance for a lumped rate constant to include both processes of excitation and deexcitation.

The lower excitation rates suggest that burnout of HCl is not a serious concern, and indeed the excitations provide ample pumping to permit excellent fits to laser energy extraction, as illustrated in Sec. III. The next question is whether the attachment driven by this excitation is adequate to calculate the electron densities measured by Kimura *et al.*[12] Extensive simulations and analysis of these results were performed and have been previously reported.[133] In summary, for moderate and high initial HCl concentrations, the model predicts values of the electron density that are within

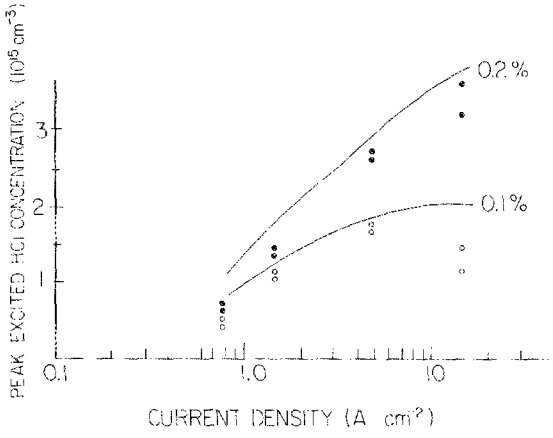

FIG. 16. Data (points) and model simulations (solid lines) for peak values of excited HCl concentration ($\times10^{15}$ cm^{-3}) vs pumping e-beam current (A cm^{-2}) measured in the experiment of Center *et al.* (Ref. 132). Open points are for 0.1% initial concentration of HCl in 1 atm of argon; closed points are for 0.2% initial concentration.

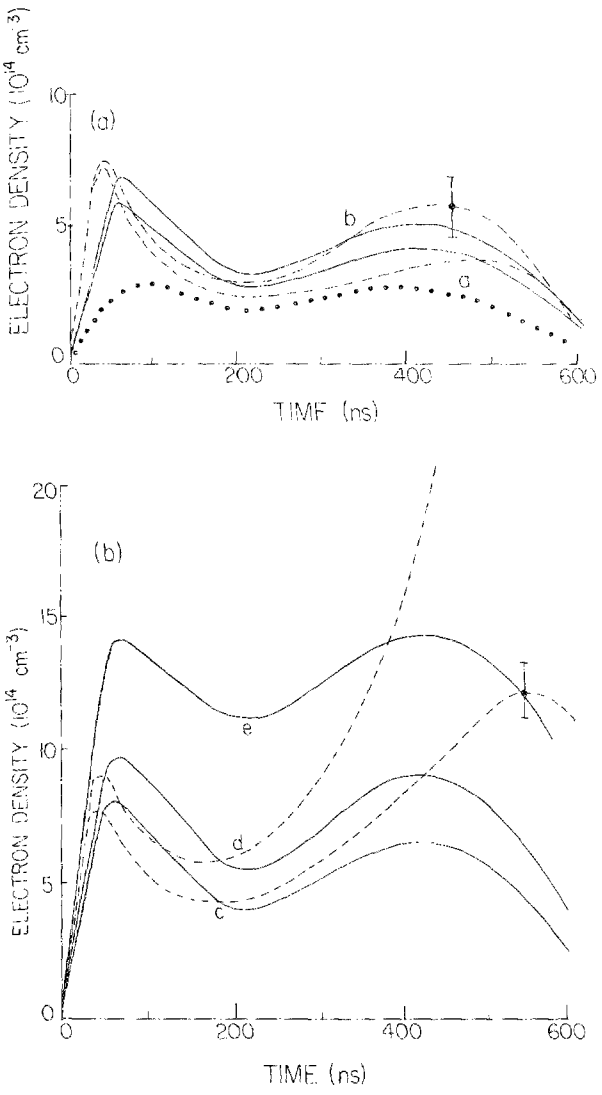

FIG. 17. Data (dashed lines) and model simulations (solid lines) for measurements of electron density ($\times 10^{14}$ cm^{-3}) vs *e*-beam pulse time (ns) in the experiments of Kimura *et al.* (Refs. 12 and 133). Total pressure was 3000 Torr with neon buffer gas. (a) Curves for initial HCl concentrations of (a) 0.2% and (b) 0.16%, and a representative *e*-beam pulse shape (shown with points). Note error bar from experimental paper; all the simulation points lie within the error bars. (b) Curves for initial HCl concentrations of (c) 0.12% and (d) 0.08%, and a simulation (e) of the same conditions in a gas with no HCl at all.

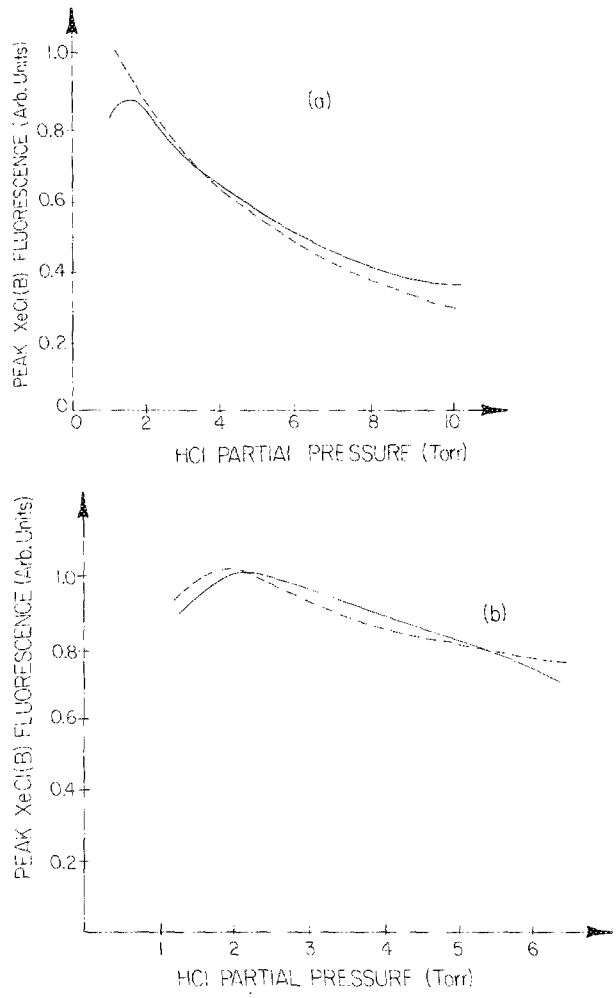

FIG. 18. Data (dashed line) and model simulations (solid line) of relative peak fluorescence from the XeCl* (B) state (arbitrary units) vs initial HCl concentration (Torr) for experiments at moderate pumping levels. (a) Experiments at Thermo Electron Technologies Corporation (Ref. 135). (b) Experiments at Spectra Technologies, Inc. (Ref. 136).

the experimental error bars at every point throughout the pulse [Fig. 17(a)]. At low initial HCl concentrations, the experimental electron density curves initially retain similar shapes, but about the middle of the pulse they rise dramatically; the model calculations reproduce the first half of the pulse faithfully, but fail to predict the large increases [Fig. 17(b)]. A calculation performed with no HCl present in the neon-xenon gas [curve e in Fig. 17(b)] also fails to show the increase in electron density, suggesting that HCl depletion is not the source of such a phenomenon. Arguments presented in Ref. 133, based on both charge balance and energy balance, demonstrate that the no-HCl calculations are correct, and that the existence of such high values of electron density is questionable.

Finally, XeCl* fluorescence measurements also published by Kimura *et al.* were plotted as a function of initial HCl concentration to obtain a Stern–Vollmer plot of quenching of the upper state. Compared to predictions of the model, the data of Ref. 12 showed too steep a slope. Even correcting for artificially high electron densities at low HCl concentrations, the experimental data suggests significantly more quenching than can be accounted for by the HCl, and the model identifies the additional contribution as arising mainly from electron quenching. The rate constant for this process initially used in the model was 2.0×10^{-7} cm^3 s^{-1}, a number widely used in the community and inferred from experiments in krypton fluoride by Trainor and Jacob.[134] However, considerably lower values had later been reported by Morgan and Pound[92] and by Burnham *et al.*,[153] based on a similar analysis of their own experimental data in xenon chloride. Consequently, the authors requested that Dr. J. Oldenettel and his colleagues perform a Stern–Vollmer analysis on their XeCl device. The results of their experiment[135] are shown in Fig. 18(a), along with model simulations performed using Morgan and Pound's electron quenching rate constant of 2.0×10^{-8} cm^3 s^{-1}. The model and data agree well within experimental error, although the failure of the

TTC data to turn over at very low HCl concentrations remains unexplained. Subsequently, Dr. Kannari and his colleagues at Spectra Technologies performed a second set of fluorescence measurements, for which a Stern–Vollmer analysis differed strongly from the first set of data,[12] but agreed quite well with the model. A comparison of the new data[136] with model calculations (again using low quenching rates) is shown in Fig. 18(b). The lower electron quenching rate has therefore been adopted as an integral part of the model. It should be noted that the higher quenching rate had proliferated by analogy to other processes, such as electron quenching of rare gas-halide triatomics, both in earlier models and our own. In all these cases, the present model now uses the lower electron quenching rate.

The other major quencher of the excited XeCl molecule is atomic xenon, which through a three-body quenching process produces the major absorber Xe_2Cl^*. Laser output under some pumping circumstances can be a sensitive function of this rate constant. Measurements by Lorents, Sharpless, and Huestis[123] show a fairly strong pressure dependence to the rate constant, with a value in the vicinity of 7.0×10^{-31} $cm^6\,s^{-1}$, and perhaps as high as 1.0×10^{-30} $cm^6\,s^{-1}$. The value used in the model is 5.0×10^{-31} $cm^6\,s^{-1}$, at the lower end of the measured range. But the factor-of-2 upper range produces a significant difference in predicted laser performance, in effect an inability to simulate the experiments presented in Sec. III accurately. Once again, the authors appealed to the experimental team at Thermo Electron Technologies Corporation, who performed a direct measurement of Xe_2Cl^* sidelight fluorescence.[137] The experimental pulse shape, together with the model's simulation of it (using the low rate constant), are shown in Fig. 19. Because the detector used in the experiment had a 100-nm bandwidth, it was necessary to include in the simulation

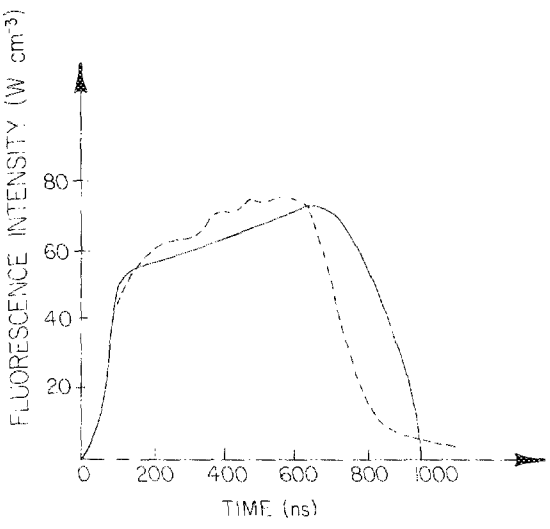

FIG. 19. Data (dashed line) and model simulations (solid line) of sidelight fluorescence (W/cm^3) in the band 500–600 nm vs time (ns) measured during lasing experiments similar to those shown in Figs. 9 and 10 performed at Thermo Electron Technologies Corporation (Ref. 137). Principal radiation in this band is from Xe_2Cl^*, with smaller contributions from xenon and neon metastable states.

spontaneous line radiation from excited atomic states of xenon and neon for those particular states that lay within the detector's acceptance. The excellent agreement of the model both with the magnitude of the fluorescence signal and the shape of the pulse suggest that the value of 5.0×10^{-31} $cm^6\,s^{-1}$ is appropriate for lasing conditions; substitution of 7.0×10^{-31} $cm^6\,s^{-1}$ substantially degraded the agreement with these measurements.

Another topic that has received considerable study and debate is the question of dissociation of the lower laser level, $XeCl(X)$. Like the ground state of XeF, the X state in XeCl is bound; but unlike XeF, it is weakly bound: roughly 250 cm^{-1}, or about kT at room temperature. Thus one would expect bottlenecking to be less of a problem for XeCl than for XeF. A direct measurement of the decay of the X state by collisions with various heavy molecules and atoms was made in 1979 by Waynant and Eden.[107] Their measurement suggested that although the rate constant for quenching by HCl is relatively high (2.0×10^{-11} $cm^3\,s^{-1}$), the rate constants for quenching by xenon and neon are considerably lower (6.0×10^{-12} and 1.0×10^{-13} $cm^3\,s^{-1}$, respectively). In typical neon-buffered laser mixtures, this would make xenon the most effective quencher, with an X state lifetime of roughly 15 ns.

However, such a long lifetime proved impossible to correlate with laser experiments in either simple or complex kinetic models. Levin *et al.*[1] chose a rate corresponding to an X state lifetime of about 1 ns, and Kannari *et al.*[2] chose to model the process with a 200 ps lifetime rather than a rate equation. Burnham *et al.*[59] at the Naval Research Laboratory assumed a lifetime of "<0.5 ns" in their kinetic model. However, they independently measured the decay of the X state, and concluded experimentally that the lifetime was approximately 1 ns. The present model uses a kinetic rate constant of 8.0×10^{-12} $cm^3\,s^{-1}$ for collisions with all rare-gas atoms; in neon buffers, this is equivalent to about a 1.3 ns lifetime. Including the reverse reaction reconstituting $XeCl(X)$,[108] the net lifetime is close to 1 ns, a value that provides accurate simulations of lasing and scaling across the range of extant data.

A final kinetic process deserving specific mention is absorption of 308 nm photon by photoassociation of xenon and chlorine atoms, viz.,

$$Xe + Cl + h\nu \rightarrow XeCl^*.$$

This is an extraction loss since, although the absorption does result in a new upper state, the process effectively doubles the time for quenching of that state. Numerous theoretical estimates[138] of a cross section for this process have been made with more than an order of magnitude span from roughly 1.0×10^{-38} to 5.0×10^{-37} cm^2. The general effect of changing this cross section is to raise or lower curves of energy delivered in lasing calculations without significantly changing their shape. Because of this, and because of the large uncertainty in its value, this cross section was used as the final free parameter in tuning the code that employs this model. That is, once other values had been fixed by direct experiment or, as just described above, by combinations of experiments and inference, the value for the photoassocia-

tion cross section was chosen as 5.0×10^{-38} cm^2 because that value gave the best fit to the Sandia lasing data.[27] That cross section—and all the other rates and cross sections in the code— were held fixed for all subsequent simulations.

ACKNOWLEDGMENTS

This model is the product of several years' development and refinement; during the course of the development, many people made substantial contributions of advice, calculations, and experiments. The authors particularly wish to acknowledge the continual wisdom and ready helpfulness of Dr. D. L. Huestis and Dr. D. C. Lorents of SRI International, and the experimental acumen and cooperative spirit of Dr. K. Y. Tang and Dr. J. Oldenettel of Thermo Electron Technologies.

APPENDIX: CALCULATION OF THE STIMULATED EMISSION AND ABSORPTION CROSS SECTION

Our starting points are the definitions of $\sigma_S(\nu)$ and $\sigma_A(\nu)$ given in Eqs. (6) and (7) of Sec. II. In evaluating these expressions, approximate descriptions of the vibrational and rotational energy level structures of the B and X states have been taken from the literature.[16,17] For the X state, the vibrational energy levels are

$$G''(V'') = 26.22X + 0.321X^2 + 0.0853X^3 + 0.00191X^4, \tag{A1}$$

where $X \equiv (V'' + \frac{1}{2})$. (All energies will be given in cm^{-1}.) For a given vibrational level, the rotational energy levels may be approximated by[18]

$$F''_{e,f}(N'') = B''K''_{e,f} - D''(K''_{e,f})^2 + H''(K''_{e,f})^3, \tag{A2}$$

where

$$K''_e = N''(N''+1) + \alpha N'',$$
$$K''_f = N''(N''+1) - \alpha(N''+1). \tag{A3}$$

We use the notation of Tellinghuisen *et al.*,[19] i.e., B'', D'', and H'' are the rotational constant and centrifugal distortion constants, respectively; N'' is the rotational quantum number; and e and f denote the two spin components for each N''. In terms of the total angular momentum J'', Eqs. (A3) take the form

$$K''_e = (J'' - \tfrac{1}{2})(J'' + \tfrac{1}{2}) + \alpha(J'' - \tfrac{1}{2}),$$
$$K''_f = (J'' + \tfrac{1}{2})(J'' + \tfrac{3}{2}) - \alpha(J'' + \tfrac{3}{2}), \tag{A4}$$

where the allowable values of J'' are $J'' = \frac{1}{2},\frac{3}{2},\frac{5}{2},\ldots$.

The splitting constant $\alpha \simeq 0.4$ for the X state. The constants B'', D'', H'' are in general functions of the vibrational quantum number V'', and are given in Ref. 2 for $V'' = 0$ and $V'' = 12$:

$V'' = 0$:

$$B'' = 0.56, \quad D'' = 9.3\times10^{-7},$$
$$H'' = -2.0\times10^{-11};$$

$V'' = 12$:

$$B'' = 0.0274, \quad D'' = 1.9\times10^{-6},$$
$$H'' = -1.8\times10^{-10}. \tag{A5}$$

For values of V'' between 0 and 12, we estimated the values of B'', D'', and H'' from the values in (A5) by interpolation.

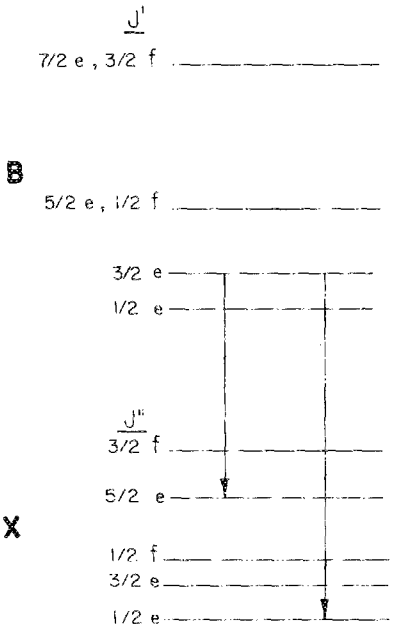

FIG. 20. Schematic rotational energy level diagrams for the B and X states of XeCl, showing allowed transitions out of the $J' = \frac{3}{2}e$ upper level.

For the B state, the vibrational energy can be approximated by

$$G'(V') = 194.75Y - 0.627Y^2, \tag{A6}$$

where $Y \equiv (V' + \frac{1}{2})$. The rotational levels are[20,21]

$$F'(K'_{e,f}) = B'K'_{e,f} - D'(K'_{e,f})^2, \tag{A7}$$

where

$$K'_e = J'(J'+1) - \tfrac{1}{2} - \delta(J' + \tfrac{1}{2}),$$
$$K'_f = J'(J'+1) - \tfrac{1}{2} + \delta(J' + \tfrac{1}{2}), \tag{A8}$$

with $J' = \frac{1}{2},\frac{3}{2}\ldots$ being the allowable values of the total angular momentum. The estimated value of the splitting constant δ from Ref. 18 is 2.0, and the constants B' and D' are given for $V' = 0$ as $B' = 0.0669$ and $D' = 3.2\times10^{-8}$. In the absence of more detailed spectroscopic information, we take these constants to be independent of V'.

The resulting energy level structure is shown schematically in Fig. 20, along with the allowable transitions out of the XeCl(B) $J' = \frac{3}{2}e$ state. We note here that the e and f designations denote states with parity $+(-1)^{J-\frac{1}{2}}$ and $-(-1)^{J-\frac{1}{2}}$, respectively,[20] so that the parity selection rule ($+ \rightarrow -$, $- \rightarrow +$) and the angular momentum selection rule ($\Delta J = \pm 1$) are consistent with transitions only between states of like (e or f) designation. We note also that $\delta = 2.0$ results in a degeneracy between e and f states with values of J' which differ by 2.

Having described the B and X level structures, we now proceed to the calculation of the desired cross sections. For the stimulated emission cross section we require the partition function Q' obtained by summing over the levels of the B state:

$$Q' = \sum_{V'}\sum_{e,f}\sum_{J'}(2J'+1)e^{-[G'(V')+F'(J')]hc/kT}, \tag{A9}$$

where we have indicated explicitly the sum over both e and f levels. The sum in (A9) extends over all bound vibrational

and rotational levels, i.e., those levels which satisfy the condition

$$D'_e - [G'(V') + F'(J')] > 0, \tag{A10}$$

where $D'_e = 36\,553\ \mathrm{cm}^{-1}$ is the dissociation energy. The stimulated emission cross section at wave number ν is then given by

$$Q'\sigma_s(\nu) = \frac{\lambda^2}{8\pi\tau} \sum_{V'} \sum_{V''} \sum_{ef} \sum_{J'} \sum_{P,R} \begin{bmatrix} J'+1 \\ J' \end{bmatrix} \times S(\nu - \tilde{\nu}) e^{-[G'(V') + F'(J')]hc/kT},$$

$$\tilde{\nu} = \begin{cases} \Delta T_e + G'(V') - G''(V'') + F'(J') - F''(J'+1) \\ \qquad (P \text{ branch}), \\ \Delta T_e + G'(V') - G''(V'') + F'(J') - F''(J'-1) \\ \qquad (R \text{ branch}). \end{cases} \tag{A11}$$

The electronic energy difference ΔT_e is approximately $32\,450\ \mathrm{cm}^{-1}$. In the numerical evaluation of (A11), we estimated the required Franck–Condon factors by interpolation from the values given in Table V of Ref. 16. Numerical results are shown in Fig. 2 for the wavelength range 3065–3095 Å.

The calculation of the absorption cross section proceeds along similar lines—the partition function Q'' is of course obtained by summation over X state levels, with the condition

$$D''_e - [G''(V'') + F''(J'')] > 0, \tag{A12}$$

where $D''_e = 281\ \mathrm{cm}^{-1}$, and the argument of the exponential in (A11) is replaced by $[G''(V'') + F''(J'')]hc/kT$. Numerical results for $\sigma_A(\nu)$ are also shown in Fig. 2.

[1]L. A. Levin, S. E. Moody, E. L. Klostermann, R. E. Center, and J. J. Ewing, IEEE J. Quantum Electron. **QE-17**, 2282 (1981).
[2]F. Kannari, A. Suda, M. Obara, and T. Fujioka, IEEE J. Quantum Electron. **QE-19**, 1587 (1983).
[3]J. J. Ewing and C. A. Brau, Appl. Phys. Lett. **27**, 350 (1975).
[4]G. C. Tisone and J. M. Hoffman, Appl. Phys. Lett. **39**, 145 (1981); IEEE J. Quantum Electron. **QE-18**, 1008 (1982).
[5]S. E. Moody, L. A. Levin, R. E. Center, J. J. Ewing, and E. L. Klostermann, IEEE J. Quantum Electron. **QE-17**, 1856 (1981).
[6]D. E. Rothe, J. B. West, and M. L. Bhaumik, IEEE J. Quantum Electron. **QE-15**, 314 (1979).
[7]L. F. Champagne, Appl. Phys. Lett. **33**, 523 (1978).
[8]R. O. Hunter, K. Tang, and J. Oldenettel (private communication). Data from these experiments is shown in Figs. 8 and 9.
[9]L. Litzenberger, R. Slater, and D. Trainor, in *Proceedings of the International Conference on Lasers '85*, edited by C. P. Wang (STS, McLean, VA, 1986), p. 573.
[10]T. H. Johnson and A. M. Hunter, J. Appl. Phys. **51**, 2406 (1980).
[11]R. E. Center, J. H. Jacob, M. Rokni, and Z. Rozenberg, Appl. Phys. Lett. **41**, 116 (1982).
[12]W. D. Kimura, D. R. Guyer, S. E. Moody, J. F. Seamans, and D. H. Ford, Appl. Phys. Lett. **49**, 1569 (1986).
[13]D. R. Guyer, W. D. Kimura and S. E. Moody, in *Proceedings of the International Conference on Lasers '86*, edited by R. W. McMillan (STS, McLean, VA, 1987), p. 589.
[14]K. Y. Tang and J. Oldenettel (private communication). Data from these experiments is shown in Figs 18(a) and 19.
[15]P. J. Hay and T. H. Dunning, Jr., J. Chem. Phys. **69**, 2209 (1978).
[16]A. Sur, A. K. Hui, and J. Tellinghuisen, J. Molec. Spectrosc. **74**, 465 (1979).
[17]J. Tellinghuisen, J. M. Hoffman, G. C. Tisone, and A. K. Hays, J. Chem. Phys. **64**, 2484 (1976).
[18]G. Herzberg, *Spectra of Diatomic Molecules* (Van Nostrand, Princeton, NJ, 1950).
[19]J. Tellinghuisen, P. C. Tellinghuisen, G. C. Tisone, J. M. Hoffman, and A. K. Hays, J. Chem. Phys. **68**, 5177 (1978).
[20]I. Kopp and J. T. Hougen, Can. J. Phys. **45**, 2581 (1967).
[21]L. Veseth, J. Phys. B **6**, 1473 (1973).
[22]V. A. Adamovich, V. Yu. Baranov, A. A. Deryugin, I. V. Kochetov, D. D. Malyuta, A. P. Napartovich, Yu. B. Smakovskii, and A. P. Strel'tsov, Sov. J. Quantum Electron. **17**, 45(1987).
[23]O. L. Bourne and A. J. Alcock, Appl. Phys. Lett. **42**, 777 (1983); R. S. Taylor, P. B. Corkum, S. Watanabe, K. E. Leopold, and A. J. Alcock, IEEE J. Quantum Electron. **QE-19**, 416 (1983).
[24]C. B. Collins and F. W. Lee, J. Chem. Phys. **72**, 5381 (1980).
[25]L. E. Christophorou and J. A. D. Stockdale, J. Chem. Phys. **48**, 1956 (1968).
[26]M. Allan and S. F. Wong, J. Chem. Phys. **74**, 1687 (1981).
[27]G. C. Tisone and J. M. Hoffman, Appl. Phys. Lett. **39**, 145 (1981); IEEE J. Quantum Electron. **QE-18**, 1008 (1982).
[28]G. C. Tisone (private communication). Dr. Tisone could not provide a quantitative experimental uncertainty, but asserted that the calculations shown in Fig. 7 lay within his own estimate of the uncertainty of his measurements.
[29]K. Y. Tang and J. Oldenettel (private communication).
[30]L. Litzenberger, R. Slater, and D. Trainor, in *Proceedings of the International Conference on Lasers '85*, edited by C. P. Wang (STS, McLean, VA, 1986), p. 573.
[31]D. C. Lorents, Physica **82C**, 19 (1976).
[32]Calculations by J. Comly, Los Alamos National Laboratory, reported in A. M. Hunter, R. O. Hunter, and T. H. Johnson, IEEE J. Quantum Electron. **QE-22**, 386 (1986).
[33]M. J. Berger and S. M. Seltzer, "Tables of Energy Loss and Ranges of Electrons and Positrons," NASA Report No. SP-3012 (1964).
[34]R. E. Center, J. H. Jacob, M. Rokni, and Z. Rozenberg, Appl. Phys. Lett. **41**, 116 (1982).
[35]W. L. Nighan and R. T. Brown, Appl. Phys. Lett. **36**, 498 (1980).
[36]M. Allan and S. F. Wong, J. Chem. Phys. **74**, 1687 (1981).
[37]C. J. Howard, F. C. Fehsenfeld, and M. McFarland, J. Chem. Phys. **60**, 5086 (1974).
[38]M. Rokni, J. Jacob, and J. Mangano, Appl. Phys. Lett. **34**, 187 (1979).
[39]L. A. Levin, S. E. Moody, E. L. Klostermann, R. E. Center, and J. J. Ewing, IEEE J. Quantum Electron. **QE-17**, 2282 (1981).
[40]D. L. Huestis, in *Proceedings of the International Conference on Lasers '85*, edited by C. P. Wang (STS, McLean, VA, 1986).
[41]F. Kannari, A. Suda, M. Obara, and T. Fujioka, IEEE J. Quantum Electron. **QE-19**, 1587 (1983).
[42]J. N. Bardsley and M. A. Biondi, Adv. At. Molec. Phys. **6**, 2 (1970).
[43]Y. Shio, M. Biondi, and D. Sipler, Phys. Rev. A **15**, 494 (1977).
[44]L. Frommhold, M. Biondi, and F. Mehr, Phys. Rev. **165**, 44 (1968).
[45]R. H. Neynaber and S. Y. Tang, J. Chem. Phys. **70**,4272 (1979).
[46]D. L. Huestis, R. M. Hill, H. H. Nakano, D. C. Lorents, J. Chem. Phys. **69**, 5133 (1978).
[47]J. B. Laudenslager, in *Kinetics of Ion-Molecule Reactions*, edited by P. Auslous (Plenum, New York, 1979).
[48]Estimated by D. C. Lorents (private communication).
[49]D. W. Setser, presented at a workshop on Kinetic Processes in Rare Gas Halide Lasers, at the 30th Gaseous Electronics Conference, Palo Alto, CA, October, 1977 (unpublished).
[50]C. A. Brau, in *Excimer Lasers*, edited by C. K. Rhodes (Springer, New York, 1984).
[51]P. K. Leichner and R J. Ericson, Phys. Rev. A **9**, 251 (1974).
[52]D. C. Lorents, D. J. Eckstrom, and D. Huestis, "Excimer Formation and Decay Processes in Rare Gases," SRI Report No. MP 73-2, SRI International, Menlo Park, CA (September, 1973).
[53]A. P. Vitols and H. J. Oskam, Phys. Rev. A **8**, 1860 (1973).
[54]D. Smith and P. R. Cromey, J. Phys. B **1**,638 (1968).
[55]W. C. F. Liu and D. C. Conway, J. Chem. Phys. **62**, 3070 (1975).
[56]A. P. Vitols and H. J. Oskam, Phys. Rev. A **5**, 2618 (1972).
[57]T. G. Finn, L. J. Palumbo, and L. F. Champagne, Appl. Phys. Lett. **33**, 148 (1978).
[58]D. L. Huestis, D. J. Eckstrom, B. E. Perry, R. M. Hill, W. K. Bischel, K. Y. Tang, and D. C. Lorents, "Electronic Transition Laser Systems," SRI Report No. MP81-04, SRI International, Menlo Park, CA (March, 1981).
[59]R. Burnham, L. F. Champagne, R. S. F. Chang, R. W. Waynant, L. J. Palumbo, and N. Djeu, "DARPA-NRL Laser Program Annual Techni-

cal Report," NRL Memorandum Report No. 4768, U.S. Naval Research Laboratory, Washington, DC (March, 1982).
[60]R. J. Shul, R. Passarella, B. L. Upschulte, R. G. Keesee, and A. W. Castleman, Jr., J. Chem. Phys. **86**, 4446 (1987).
[61]By analogy to T. G. Finn, L. J. Palumbo, and L. F. Champagne, Appl. Phys. Lett. **33**, 148 (1978).
[62]J. Bokov and C. K. Rhodes, J. Chem. Phys. **73**, 2626 (1980).
[63]C. B. Collins and F. W. Lee, J. Chem. Phys. **72**, 5381 (1980).
[64]Analogy with S. J. Nagalingam and G. H. Miley, in the IEEE-OSA Topical Meeting on Excimer Lasers, Charleston, SC (September, 1979) (unpublished).
[65]H. J. Kramer, J. A. Herce, and E. E. Muschlitz, J. Chem. Phys. **56**, 4166 (1972).
[66]Analogy with M. A. Biondi, Phys. Rev. **129**, 1181 (1963).
[67]N. Basov, E. P. Glotov, V. S. Danilychev, A. I. Milanich, and A. M. Soroka, Sov. Tech. Phys. Lett. **5**, 183 (1979).
[68]J. B. Hoffman and J. B. Moreno, "Three-body ion-ion recombination coefficients for rare gas halogen mixtures," Sandia National Laboratory Report No. SAND80-1486, Sandia Laboratories, Albuquerque, NM (August, 1980).
[69]R. S. F. Chang, J. Chem. Phys. **76**, 2943 (1982).
[70]Analogy with J. H. Kolts, J. E. Velazco, and D. W. Setser, J. Chem. Phys. **71**, 1247 (1979).
[71]Estimated by L. A. Levin, S. E. Moody, E. L. Klostermann, R. E. Center, and J. J. Ewing, IEEE J. Quantum Electron. **QE-17**, 2282 (1981).
[72]D. L. Huestis, R. M. Hill, D. J. Eckstrom, M. V. McCusker, D. C. Lorents, H. H. Nakano, B. E. Perry, J. A. Margevicius, and N. E. Schlotter, SRI Report No. MP78-07, SRI International, Menlo Park, CA (May, 1978).
[73]J. H. Kolts and D. W. Setser, in the 7th Winter Colloquium on High Power Visible Lasers, Park City, UT, 1977 (unpublished).
[74]J. K. Rice and A. W. Johnson, J. Chem. Phys. **63**, 5235 (1975).
[75]P. K. Leichner, K. F. Palmer, J. D. Cook, and M. Thieneman, Phys. Rev. A **13**, 1787 (1976).
[76]P. R. Timpson and J. M. Anderson, Can. J. Phys. **48**, 1817 (1970).
[77]H. H. Nakano, R. M. Hill, D. C. Lorents, D. L. Huestis, M. V. McCusker, and D. J. Eckstrom, SRI Report No. MP 76-99, SRI International, Menlo Park, CA (1976).
[78]Y. J. Shiu, M. A. Biondi, and D. P. Sipler, Phys. Rev. A. **15**, 494 (1977).
[79]Y. J. Shiu and M. A. Biondi, Phys. Rev. A **16**, 1817 (1977).
[80]K. T. Gillen, R. P. Saxon, D. C. Lorents, G. E. Ice, and R. E. Olson, J. Chem. Phys. **64**, 1925 (1976).
[81]J. E. Velazco, J. H. Kolts, and D. W. Setser, J. Chem. Phys. **65**, 3468 (1976).
[82]M. Bourene and J. LeCalye, J. Chem. Phys. **58**, 1452 (1973).
[83]L. G. Piper, J. E. Velazco, and D. W. Setser, J. Chem. Phys. **59**, 3323 (1973).
[84]F. Kannari, A. Suda, M. Obara, and T. Fujioka, IEEE J. Quantum Electron. **QE-19**, 1587 (1983).
[85]R. E. Gleason, T. D. Bonifield, J. W. Keto, and G. K. Walters, J. Chem. Phys. **66**, 1589 (1977).
[86]Analogy with N. Sadeghi and J. Sabbagh, Phys. Rev. A **16**, 2336 (1977).
[87]H. C. Brashears, D. W. Setser, and Y. C. Yu, J. Chem. Phys. **84**, 2495 (1980).
[88]Analogy with H. H. Nakano, R. M. Hill, D. C. Lorents, D. L. Huestis, M. V. McCusker, and D. J. Eckstrom, SRI Report No. MP 76-99, SRI International, Menlo Park, CA (1976).
[89]G. P. Glass, F. K. Tittel, W. L. Wilson, M. S. Smayling, and G. Marowsky, Chem. Phys. Lett. **83**, 585 (1981).
[90]C. H. Fisher, R. E. Center, and J. P. McDaniel, in the 32nd Annual Gaseous Electronics Conference, Pittsburgh, PA, October, 1979 (unpublished).
[91]T. G. Finn, R. S. F. Chang, L. J. Palumbo, and L. F. Champagne, Appl. Phys. Lett. **36**, 789 (1980).
[92]W. L. Morgan and M. J. Pound, in the 33rd Annual Gaseous Electronics Conference, Norman, OK, October, 1980(unpublished).
[93]G. C. Tisone and J. M. Hoffman, Appl. Phys. Lett. **39**,145 (1981).
[94]G. C. Tisone and J. M. Hoffman, "Study of the XeCl Laser Pumped by a High-Intensity Electron Beam," Sandia Report No. SAND 81-1890J, Sandia National Laboratories, Albuquerque, NM (1981).
[95]D. C. Lorents and R. E. Olson, "Excimer Formation and Decay Processes in Rare Gases," SRI Semi-Annual Technical Report for contract No. N00014-72-C-0457, SRI International, Menlo Park, CA (December, 1972).
[96]J. H. Kolts, J. E. Velazco, and D. W. Setser, J. Chem. Phys. **71**, 1247 (1979).
[97]F. K. Tittel, G. Marowsky, W. L. Wilson, and M. C. Smayling, IEEE J. Quantum Electron. **QE-17**, 2268 (1981).
[98]Analogy with P. J. Hay and T. H. Dunning, J. Chem. Phys. **69**, 2209 (1978).
[99]D. W. Setser, H. C. Brashears, and T. D. Dreiling, J. Phys. (Paris) **41**, C3-195 (1980).
[100]K. Y. Tang and D. C. Lorents, in *Proceedings of the International Conference on Lasers '81* (STS, McLean, VA, 1981).
[101]A. Mandl, Phys. Rev. A **14**, 345 (1976).
[102]E. Zamir, D. L. Huestis, H. H. Nakano, R. M. Hill, and D. C. Lorents, IEEE J. Quantum Electron. **QE-15**, 281 (1979).
[103]F. Collier, J. B. Leblond, F. Hoffbeck, and P. Cottin, J. Chem. Phys. **74**, 4372 (1981).
[104]G. Inoue, J. Ku, and D. W. Setser, J. Chem. Phys. **80**, 6006 (1984).
[105]P. J. Hay and T. H. Dunning, J. Chem. Phys. **69**, 2209 (1978).
[106]M. P. Grieneisen, H. Xue-Ting, and K. L. Kompa, Chem. Phys. Lett. **82**, 441 (1981).
[107]R. W. Waynant and J. G. Eden, Appl. Phys. Lett. **36**, 262 (1980).
[108]K. Y. Tang and D. L. Huestis, "Calculations of Equilibrium Constants of $XeCl \rightleftarrows Xe + Cl$ Between 200 and 500 K," SRI Technical Report No. MP 79-82, SRI International, Menlo Park, CA (October, 1979).
[109]W. R. Wadt, J. Chem. Phys. **73**, 3915 (1980).
[110]H. H. Michels, R. H. Hobbs, and L. A. Wright, Int. J. Quant. Chem. **12**, 257 (1978).
[111]H. H. Michels and R. H. Hobbs, J. Chem. Phys. **71**, 5053 (1979).
[112]R. H. Neynaber and S. Y. Tang, Phys. Rev. A **23**, 611 (1981).
[113]T. Oka, M. Kogoma, M. Imarura, S. Araj, and T. Watanabe, J. Chem. Phys. **70**, 3384 (1979).
[114]R. E. Gleason, T. D. Bonifield, J. W. Keto, and G. K. Walters, J. Chem. Phys. **66**, 1589 (1977).
[115]J. D. C. Jones, D. G. Lister, and N. D. Twiddy, Chem. Phys. Lett. **70**, 575 (1980).
[116]W. P. West, T. B. Cook, F. B. Dunning, R. D. Rundel, and R. F. Stebbings, J. Chem. Phys. **63**, 1237 (1975).
[117]C. Duzy and H. A. Hyman, Phys. Rev. A **22**, 1878 (1980).
[118]J. J. Ewing, in *Laser Handbook*, edited by M. L. Stitch (North-Holland, Amsterdam, 1979).
[119]K. J. McCann and M. R. Flannery, Appl. Phys. Lett. **31**, 599 (1977).
[120]D. J. Seery and D. Britton, J. Phys. Chem. **68**, 2263 (1964).
[121]C. F. Bender and N. M. Winter, Appl. Phys. Lett. **33**, 29 (1978).
[122]Y. Tanaka, Y. Yoshino, and D. E. Freeman, J. Chem. Phys. **62**, 4484 (1975).
[123]D. C. Lorents, R. L. Sharpless, and D. L. Huestis, in the 39th Annual Gaseous Electronics Conference, Madison, WI, October 1986 (unpublished).
[124]E. W. McDaniel, V. Cermak, A. Dalgarno, E. E. Ferguson, and L. Friedman, *Ion Molecule Reactions* (Wiley-Interscience, New York, 1970).
[125]J. B. Gerardo and A. W. Johnson, J. Chem. Phys. **59**, 1738 (1973).
[126]D. L. Huestis, G. Marowsky, and F. K. Tittel, in *Excimer Lasers*, edited by C. K. Rhodes (Springer, New York, 1984).
[127]A. W. McCown and J. G. Eden, J. Chem. Phys. **81**, 2933 (1984).
[128]B. C. Garrett, L. T. Redman, and M. J. Redman, Phys. Rev. A **33**, 2091 (1986).
[129]T. H. Johnson, L. J. Palumbo, and A. M. Hunter, IEEE J. Quantum Electron. **QE-15**, 289 (1979).
[130]S. Leone, J. Phys. Chem. Ref. Data **11**, 953 (1982).
[131]Numerous experiments have been performed to measure or infer various values of the cross section (as a function of electron energy) for electron-impact vibrational excitation of HCl. Several authors have convolved these fragmentary results with interactive solutions of the Boltzmann equation. The cross sections used in the current analysis have relied upon calculations performed by D. K. Davis and presented at the Gaseous Electronics Conference in 1981, and upon the measurements of K. Rohr and F. Linder [J. Phys. B **9**, 2521 (1976)] and of R. E. Center and H. L. Chen [J. Chem. Phys. **61**, 3785 (1974)].
[132]R. E. Center, J. H. Jacob, M. Rokni, and Z. Rozenberg, Appl. Phys. Lett. **41**, 116 (1982).
[133]T. H. Johnson and H. E. Cartland, Appl. Phys. Lett. **52**, 1862 (1988).
[134]D. W. Trainor and J. H. Jacob, Appl. Phys. Lett. **37**, 675 (1980).
[135]K. Y. Tang and J. Oldenettel (private communication).
[136]F. Kannari (private communication).
[137]K. Y. Tang and J. Oldenettel (private communication).
[138]Calculations have been provided by private communication by D. L. Huestis, SRI International, Menlo Park, CA and S. E. Moody, Spectra

Technologies Inc., Seattle, WA. The process is discussed in G. Inoue, J. K. Ku, and D. W. Setser, J.Chem. Phys. **80**, 6006 (1984).
[139]J. H. Jacob and J. A. Mangano, Appl. Phys. Lett. **29**, 467 (1976).
[140]E. Eggarter, J. Chem. Phys. **62**, 833 (1975).
[141]M. Shaper and H. Scheibner, Beit. Plasma Phys. **9**, 45 (1969).
[142]J. H. Jacob and J. A. Mangano, Appl. Phys. Lett. **28**, 724 (1976).
[143]L. R. Peterson and J. E. Allen, J. Chem. Phys. **56**, 6068 (1972).
[144]D. Rapp and P. Englander-Golden, J. Chem. Phys. **43**, 1464 (1965).
[145]L. Vriens, Physica **31**, 395 (1965).
[146]H. A. Hyman, Phys. Rev. A **20**, 855 (1979).
[147]H. A. Hyman, Phys. Rev. A **18**, 441 (1978).
[148]J. Fletcher and I. R. Cowling, J. Phys. B **6**, L258 (1973).
[149]P. J. O. Teubner, J. L. Riley, M. C. Tonkin, J. E. Furst, and S. J. Buckman, J. Phys. B **18**, 3641 (1985).
[150]S. W. Lawton and T. A. DeTemple, "Near Infrared Gas Lasers," Technical Report No. AFAPL-TR-78-107, Air Force Wright Aeronautical Laboratories, Wright Patterson Air Force Base, OH (December, 1978).
[151]L. F. Champagne, L. J. Palumbo, and T. G. Finn, Appl. Phys. Lett. **34**, 315 (1979). Important parameters of the experimental apparatus are given in L. G. Champagne [Appl. Phys. Lett. **33**, 523 (1978)] and in L. F. Champagne, J. G. Eden, N. W. Harris, N. Djeu, and S. K. Searles [Appl. Phys. Lett. **30**, 160 (1977)].
[152]S. E. Moody, L. A. Levin, R. E. Center, J. J. Ewing, and E. L. Klostermann, IEEE J. Quantum Electron. **QE-17**, 1856 (1981).
[153]R. Burnham, L. F. Champagne, R. S. F. Chang, R. W. Waynant, L. J. Palumbo, and N. Djeu, "DARPA-NRL Laser Program Annual Technical Report," NRL Memorandum Report No. 4768, U.S. Naval Research Laboratory, Washington, DC (March, 1982), analyzing earlier experiments at the Naval Research Laboratory reported in T. G. Finn, S. F. Chang, L. F. Palumbo, and L. F. Champagne, Appl. Phys. Lett. **36**, 789 (1980).